

Article

Linking Siberian Traps LIP Emplacement and End-Permian Mass Extinction: Evidence from Magnetic Stratigraphy of the Maymecha-Kotuy Volcanic Section

Anton V. Latyshev ^{1,2,*}, Anna M. Fetisova ^{1,2} and Roman V. Veselovskiy ^{1,2} 

¹ Faculty of Geology, Lomonosov Moscow State University, 1 Leninskie Gory, 119991 Moscow, Russia; anna-fetis@yandex.ru (A.M.F.); roman.veselovskiy@ya.ru (R.V.V.)

² Schmidt Institute of the Physics of the Earth, Russian Academy of Science, 10 Bolshaya Gruzinskaya st., 123242 Moscow, Russia

* Correspondence: anton.latyshev@gmail.com

Received: 30 June 2020; Accepted: 30 July 2020; Published: 2 August 2020



Abstract: The Siberian Traps Large Igneous Provinces (LIP) emplacement is considered as one of possible triggers for the end-Permian global biotic crisis. However, relative timing of the onset of extinction and the main phase of the magmatic activity are not yet accurately constrained. We present the detailed paleomagnetic data for the thickest composite section of the Siberian Traps volcanics, located in the Maymecha-Kotuy region. The major part of the Maymecha-Kotuy section erupted in the beginning of Early Triassic period and postdate came the onset of the biotic crisis. However, the initial pulse of volcanic activity in this region took place at the end of the Permian period, and likely preceded the extinction event, being nearly coeval to the lowest part of tuff-lava sequence of Norilsk. The suggested correlation scheme of volcanic sections from different regions of the Siberian platform shows that explosive and extrusive events foregoing the onset of extinction can be identified in almost all regions of the Siberian Traps LIP. Finally, we estimate the total duration of magmatic activity in the Maymecha-Kotuy region as ~2 Myr and assume that this lasted after the termination of eruptions in other parts of the Siberian platform.

Keywords: Siberian traps; large igneous province; mass extinction; volcanic activity; magnetic stratigraphy; paleomagnetism; Maymecha-Kotuy region; Permian; Triassic

1. Introduction

Possible causal links between the global biotic crises and Large Igneous Provinces (LIP) emplacement have long been widely discussed [1–4]. It has been shown that four of so-called “big five” Phanerozoic extinctions [5] temporally coincide with formation of LIPs which represent voluminous manifestations of flood-basalt magmatic activity [6–9]. The Siberian Traps LIP is considered to be one of the largest areas of intraplate mafic magmatic activity [10–12] and is nearly coeval to the end-Permian mass extinction [13–18] which was the most severe during the Phanerozoic.

The Siberian Traps LIP comprises thick mafic tuff-lava piles and related intrusions filling up mainly the Tunguska syncline and also spreading out beyond the borders of Siberian platform (Figure 1). Within the Siberian platform, the province is subdivided into several regions with variable tectonic structure, composition, and thickness of magmatic rocks: Norilsk, Maymecha-Kotuy, Putorana, Nizhnyaya (Lower) Tunguska regions; and the Angara-Taseeva depression [19–21]. Also, products of the Permian–Triassic magmatic activity are widespread in Taymyr, West Siberian basin, Kuznetsk basin, Polar Urals, Chelyabinsk rift, Eastern Kazakhstan etc. [16,22–25]. The total volume of the

Permian–Triassic magmatic rocks within and around the Siberian platform is estimated as about $\sim 10^6\text{--}10^7$ km³ [11,26–28].

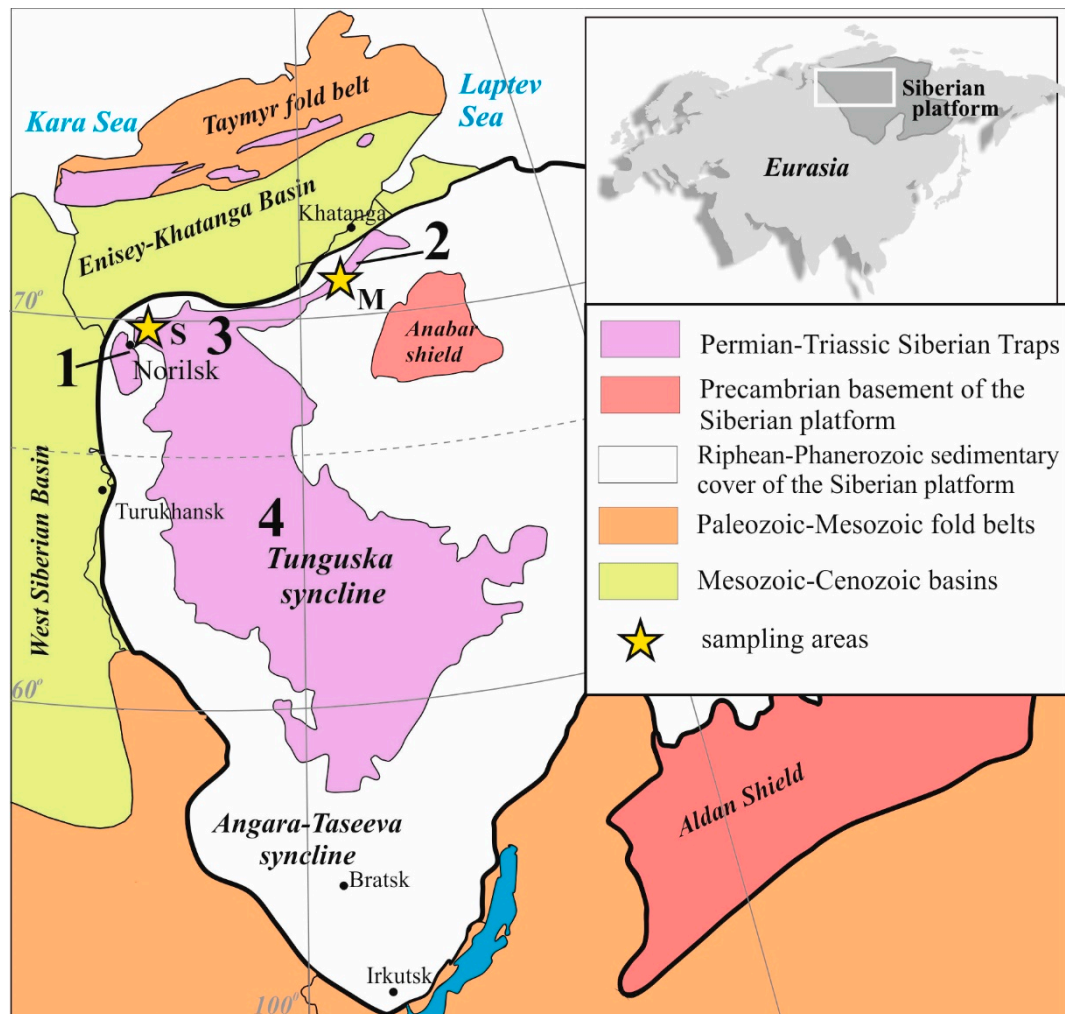


Figure 1. Geological scheme of the Siberian platform. Regions of the Siberian Traps LIP: 1—Norilsk; 2—Maymecha-Kotuy; 3—Putorana; 4—Nizhnyaya Tunguska. Sampling areas: S—Samoedsky Formation; M—Maymecha river valley.

Recent highly precise U-Pb and $^{40}\text{Ar}/^{39}\text{Ar}$ dating has shown that the main stage of extrusive and intrusive magmatic activity took place during ~ 1 Myr or even less at the very Permian–Triassic boundary [15,16,29]. However, the accurate temporal correlation of the Siberian magmatism and extinction event is still controversial because most of the reliable isotopic data on the Siberian Traps was obtained from the intrusive bodies, while the correlation of lavas and intrusions in the Siberian LIP is a special problem (e.g., [30]). The only exception is the Maymecha-Kotuy region where alkaline lavas and tuffs have been dated by U-Pb method on perovskite and zircon [15,29]. However, results of this dating are somewhat ambiguous (see below). Moreover, the correlation of the volcanic sequence of the Maymecha-Kotuy region with other areas of the Siberian Traps province is still debated as well [31–33]. Thus, it is unclear which part of the volcanic section has erupted before the biotic crisis.

In the last decades it was shown that paleomagnetic methods are very prospective for the investigation of large igneous provinces [34–37]. As to the Siberian Traps, the detailed flow-to-flow magnetic stratigraphy for the volcanic sequences of Norilsk [31,38] and Kotuy [33] was developed. Based on the analysis of the secular variations, we demonstrated that volcanic activity in the Norilsk region and the Kotuy river valley occurred as a series of brief and powerful eruptive events (“volcanic

pulses”) [39–41]. Furthermore, we suggested the scheme of correlation of the volcanic sections from various Siberian Traps regions, including the Kotuy river valley [33] and set the main intrusive events in this scheme [42]. Finally, we have recently shown that Cu-Ni-PGE bearing intrusions of the Norilsk type are coeval to the Morongovsky—Mokulaevsky formations of the volcanic section of Norilsk [30]. Since the majority of U-Pb data for the Norilsk region is obtained from intrusions of this type [14,29], this assumption has very important implications for the reconstruction of timing and duration of the Siberian Traps emplacement (see below).

In this work, we present the new paleomagnetic data from the Maymecha river volcanic section (the Maymecha-Kotuy region), suggest the scheme of correlation of this sequence with other Siberian Traps regions, and discuss the implications for the possible link between the Permian–Triassic catastrophic volcanic activity and the global biotic hazard.

Objects and Geological Background

The Maymecha-Kotuy region is located at the northern margin of the Siberian platform and forms the narrow stripe of the Permian–Triassic extrusive rocks along the southern slope of the Yenisey-Khatanga basin. The unique feature of this area is the predominance of alkaline and ultramafic rocks over tholeiitic basalts which comprise the main volume of the rest of Siberian Traps LIP [20,43]. In general, volcanic sequence of this region consists of two composite sections developed in the valleys of Maymecha and Kotuy rivers. The volcanic section of Maymecha comprises from bottom to top: mafic tuffs of the Pravoboyarsky Formation; the Kogotoksky Group (series in Russian terms), which is subdivided into the basaltic lavas of the Onkuchaksky Formation and basalts, trachybasalts, and trachyandesites of the Tyvankitsky Formation; the Delkansky Formation of highly diverse composition (from alkaline-ultramafic lavas to felsic tuffs); and picrites and meimechites of the Maymechinsky Formation [20]. The sequence of the Kotuy river valley begins with the alkaline-ultramafic tuffs known as Khardakhsky Formation [33,44] which is overlain by alkaline-ultramafic lavas of the Arydzhangsky Formation and basalts of Onkuchaksky Formation [43]. The total thickness of the composite volcanic section for the whole Maymecha-Kotuy region exceeds 3.5 km [20] and probably is the highest among the Siberian Traps. Finally, numerous dikes of variable composition and large multiphase alkaline-ultramafic plutons cut the Permian–Triassic tuff-lava pile and the Paleozoic sedimentary cover of the Siberian platform to southeast from the Maymecha-Kotuy region. Guli pluton, the largest one, intrudes the whole volcanic section of the Maymecha river, and thus represents the terminal stage of magmatic activity in this region.

Age and stratigraphic position of the tuff-lava pile relative to the Permian–Triassic boundary (PTB) is still poorly constrained. Paleontological data indicate that, in the Maymecha river area, this boundary should be set within the Pravoboyarsky Formation, due to the presence of Upper Permian spore-pollen complexes in the lower part and Lower Triassic phyllospores, in the upper part of the unit [45]. As to the Kotuy river section, Ivanov and Pirozhnikov (1959) [46] reported Upper Permian flora in the outcrops of Potokoysky Formation which are referred to as Khardakhsky Formation in this work, and Lower Triassic phyllospores in tuffaceous lenses in the middle part of the Arydzhangsky Formation. According to this data, the PTB should be placed somewhere nearby the Khardakhsky/Arydzhangsky boundary.

Kamo et al. (2003) [15] obtained U-Pb age (perovskite) of 251.7 ± 0.4 Ma from the Arydzhangsky Formation (lower part of the volcanic section). This dating is a bit younger than the onset of extinction and the PTB which are dated as 251.941 ± 0.037 Ma and 251.902 ± 0.024 Ma, respectively [47], but overlaps them within the confidence interval. On the other hand, Burgess and Bowring (2015) dated the same lava flow as 252.27 ± 0.15 Ma (here and below uncertainties for U-Pb data from [29] are given as 2σ including the systematic uncertainties associated with tracer calibration (0.03%)), that corresponds to the Late Permian and is 200–300 kyr older than the onset of biotic crisis. Besides that, Burgess and Bowring (2015) [29] reported one more age attributed to the Arydzhangsky Formation -252.2 ± 0.16 Ma, but our field data shows that this age was obtained from the sill of unclear stratigraphic position. Furthermore,

zircons from felsic tuffs and lavas of the Delkansky Formation were dated as 251.901 ± 0.089 Ma, 251.483 ± 0.11 Ma [29], and 251.1 ± 0.3 Ma [15]. Finally, baddeleyites from carbonatite stock of the youngest intrusive phase of the Guli pluton yielded U-Pb age of 250.2 ± 0.3 Ma [15].

Recently we have presented the magnetic stratigraphy of the Kotuy river tuff-lava section in detail [33]. Briefly, the volcanic sequence comprises three polarity zones, from bottom to top as follows: (1) An interval of reversed polarity that embraces the Khardakhsy Formation and likely corresponds to the lowermost Ivakinsky Formation in Norilsk tuff-lava section; (2) an interval of normal polarity that comprises the Arydzhangsky and lowermost part of the Onkuchaksky Formations and can be correlated with upper extrusive formations of the Norilsk region; (3) an interval of reversed polarity in the upper part of Onkuchaksky Formation, which is probably younger than the whole volcanic sequence of Norilsk, possibly except the uppermost Samoedsky Formation, where signs of the reversed polarity zone were reported by Gurevitch et al. (2004) [31]. However, even authors of the cited paper admitted that paleomagnetic data on the Samoedsky Formation is of poor quality and needs to be confirmed. Also, we should note that “volcanic pulses” constitute the whole tuff-lava pile of Kotuy, similarly like in the Norilsk region [41].

Paleomagnetic data, which are available for the Maymecha river volcanic section, was published more than three decades ago [48,49]. These results were obtained without the mandatory full demagnetization and component analysis, and therefore do not fit to the modern standards of quality for the paleomagnetic research. Thus, the magnetic stratigraphy of the Maymecha river valley needs revision.

Within this study, we sampled several key volcanic sections of the Maymecha river valley, representing all volcanic formations. Furthermore, we collected samples from lava flows of the uppermost Samoedsky Formation in the Verkhnyaya Talovaya river valley (Norilsk region), in order to check the information about the reversed polarity interval recorded there as suggested by Gurevitch et al. (2004) [31]. The brief description of sampling localities is given below.

Products of the Permian–Triassic magmatic activity in the Maymecha river valley constitute the volcano-tectonic depression, where the huge Guli pluton occupies the core position. Tectonic structure of the Maymecha area is quite complicated and comprises many blocks composed of different pieces of the volcanic sequence. In general, the lowermost units are exposed in the periphery of this complex volcanic edifice, changing to the upper formations towards the inner part.

Mafic tuffs of the Pravoboyarsky Formation were sampled at two locations in the Maymecha river valley, near the mouth of Balagannakh stream (profiles 1 and 2 in Figure 2A). According to the Geological Survey data [50], location 1 represents the lower unit of the Pravoboyarsky Formation, while location 2 is attributed to the upper unit. In total, 67 oriented samples were collected at 15 sites (tuff packs). The composite thickness of sampled interval is estimated as ~60 m. In addition, thin ultramafic dike (~1 m thick) cutting the Pravoboyarsky tuffs was sampled.

The Onkuchaksky Formation was sampled in the continuous section in the Maymecha river valley, near the mouth of Chopko river (profile 3 in Figure 2A). A thick packet of lava flows composed of basalts and dolerites, about 160 m thick, dips to NW or N (dip angle ~15). We have distinguished 44 flows and collected from them 186 oriented samples.

The Tyvankitsky Formation was studied at two locations: the watershed of the Maymecha and Kogotok rivers (Figure 2B; 8 lava flows mainly of trachybasaltic and trachyandesitic composition, profile 4 in Figure 2A), and the continuous outcrop at the right bank of the Maymecha river opposite to the mouth of the Kogotok river (33 lava flows and an interval without clear flow boundaries, composed of basalts and trachybasalts, profile 5 in Figure 2A). The latter section has been attributed to the Onkuchaksky Formation based on Geological Survey data [50]. However, petrographic data shows that trachybasaltic lavas occur there. Since the Onkuchaksky Formation consists of basalts only [20], we considered this section as the Tyvankitsky Formation. The top of Tyvankitsky Formation in this section is marked by the lowermost melanephelinite lava flow, which is typical of the overlying Delkansky Formation.

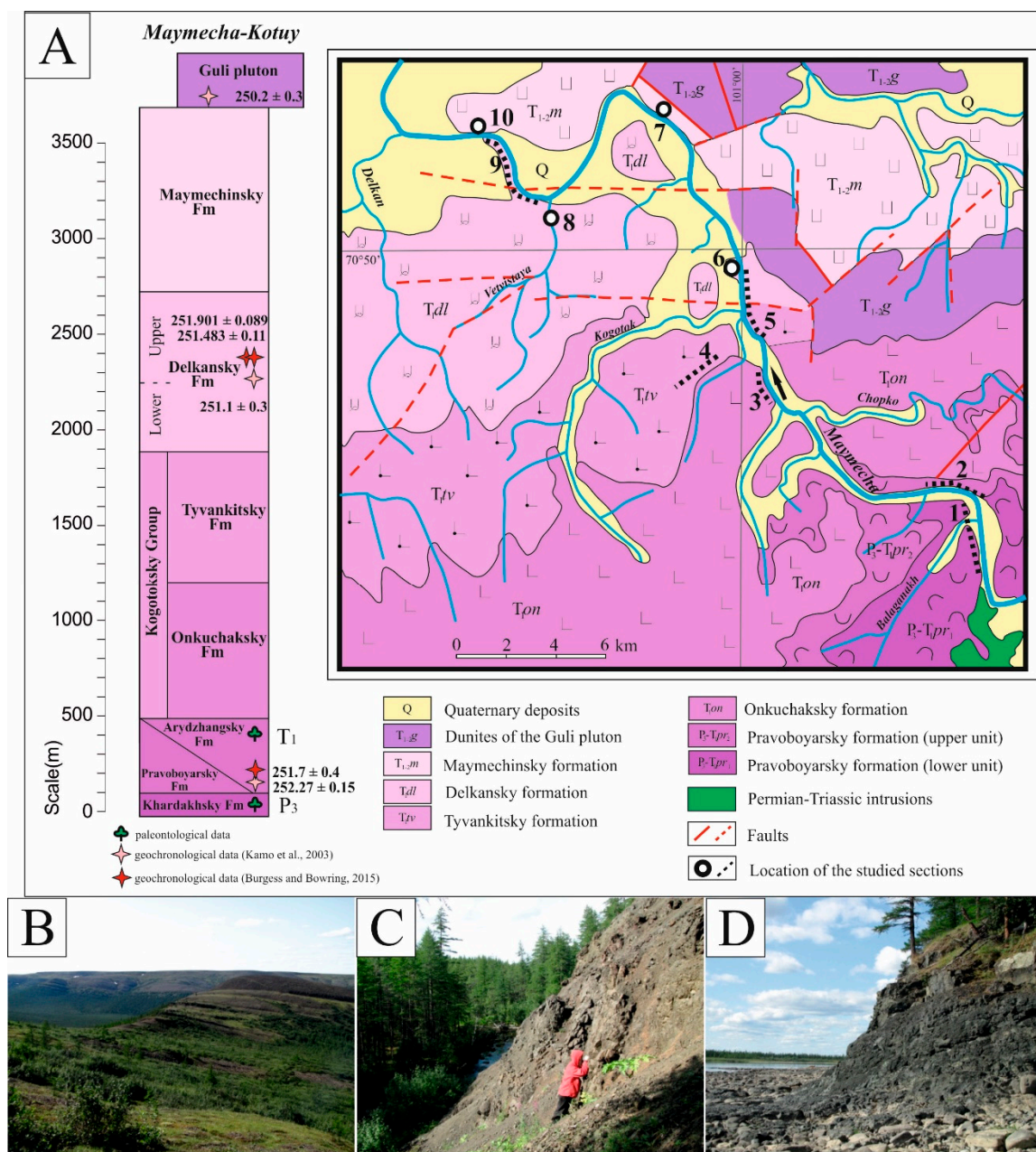


Figure 2. (A) Sketch geological map of the Maymecha river valley and the stratigraphic column of the Permian-Triassic volcanic rocks of the Maymecha-Kotuy region. (B) Lava flows of the Tyvankitsky Formation, profile 4. (C) Outcrops of the Upper Delkansky Formation lavas, the Vetvistaya river, location 8. (D) Outcrops of the Maymechinsky Formation, location 10.

We also collected samples from the Delkansky Formation in several locations (5–6 and 8–9 in Figure 2A). According to [20], this formation is subdivided to three units (“subsuites”). However, since the middle unit is poorly exposed and hardly distinguishable from the upper one in the field, in this work we subdivide the Delkansky Formation into 2 units, where the lower one corresponds to the lower subsuite, and the upper one corresponds to the middle and upper subsuites after [20]. In profile 5, eight alkaline-ultramafic lava flows of Lower Delkansky Formation, and ~90 m interval of extrusive rocks, where individual flows cannot be identified confidently, were sampled. Lava flows dip to NW with angles up to 40°, possibly due to post-magmatic block deformations. The contact with the Tyvankitsky Formation is supposed to be tectonic in this section. Location 6 represents the Lower

Delkansky unit as well and comprises lavas of variable composition and layers of presumably felsic tuffs. The whole pack plunges to the SE and reaches 15 m in thickness. 23 samples were collected from this location. Finally, upper part of the Delkansky Formation was sampled in two locations (8–9 in Figure 2A) in the Vetvistaya river valley (Figure 2C) and near its mouth. Since the volcanic pile can hardly be divided into individual flows and units, about 70 samples were collected with a step of ~1–2 m.

Ultramafic lavas of the Maymechinsky Formation were sampled at six closely located sites in outcrops 7 and 10 (Figure 2A). The outcrops represent the monotonous piles of olivine-rich meimechites and picrites without clear flow boundaries (Figure 2D). Lavas shallowly dip to NE, towards Guli pluton. In total, 35 oriented samples were collected here.

Finally, basalts of the upper part of Samoedsky Formation (uppermost in the Norilsk section) were sampled in its reference section on the right bank of the Verkhnyaya Talovaya river (the Kharaelakhsky trough of Norilsk region). Despite the poor exposure, oriented samples were collected at nine sites (individual lava flows), representing an interval of about 250 thick.

2. Methods

The oriented samples were collected as hand blocks. The orientation of samples was performed using the magnetic compass. As usual, 4–8 individual samples were collected from each lava flow or tuff layer; if it was not possible to distinguish the flow boundaries, we performed the continuous sampling with a step of about 1–1.5 m. The paleomagnetic and rock-magnetic procedures were carried out in the paleomagnetic laboratories of Schmidt Institute of Physics of the Earth (IPE RAS, Moscow, Russia) and Faculty of Geology, Lomonosov Moscow State University (Russia). All samples were subjected to the stepwise (10–18 steps) thermal treatment up to the complete demagnetization. The size of demagnetization steps was changed from 50–100 °C at low temperatures to 5–20 °C at high temperatures depending on the demagnetization pattern. For heating we used MMTD-80 non-magnetic ovens (Magnetic Measurements Ltd., Aughton, UK) with internal residual fields of about 5–10 nT. Selected specimens were demagnetized by alternating fields (AF) up to 100 mT. The remanent magnetization of samples was measured using the spinner magnetometer JR-6 (AGICO). The isolation of the natural remanent magnetization (NRM) components was performed with Enkin's [51] and Remasoft [52] paleomagnetic software packages using principal component analysis [53]. The analysis of paleomagnetic data was carried out using Fisher statistics [54].

Thermomagnetic $M_s(T)$ curves were measured using vibrating magnetometer constructed by Yu.K. Vinogradov (the Borok Geophysical Observatory, Yaroslavl region, Russia), with an applied magnetic field of 0.5 T. Thermal dependence of the magnetic susceptibility was measured using CS-3 heating add-on to the MFK-1FA kappabridge (AGICO). Electron microscopy and microprobe analysis were performed at the Borok Geophysical Observatory (analyst V.A. Tselmovich) using scanning electron microscope TESCAN VEGA II with an energy dispersive spectroscope Drycool (Oxford Instruments, Abingdon, UK).

3. Magnetic Mineralogy

We performed detailed thermomagnetic and microscopic investigation, in order to determine the composition of magnetic minerals. Magnetic mineralogy of the studied samples varies in wide ranges, due to the high diversity of rock composition. The most common features are described below.

Basalts of the Onkuchaksky Formation according to the results of the thermomagnetic analysis demonstrate the predominance of magnetite as a single magnetic phase. Thermal dependences of magnetic susceptibility ($K(T)$) and saturation magnetization ($M_s(T)$) show the sharp decrease of magnetic parameters at temperatures about 560–590 °C (Figure 3A). In some samples, some amount of hematite ($T_c = 670$ °C) or titanomagnetite ($T_c = 450$ °C) is identified at magnetic susceptibility curves. Many samples are very stable to thermal treatment: curves of heating and cooling are almost identical. Occasionally, after the heating-cooling cycle values of M_s and K decrease, possibly, due to

the presence of some amount of maghemite, which is inverted to hematite during heating (Figure 3B). Rarely, at cooling Curie temperatures come down to 500–550 °C, possibly due to the homogenization of exsolved titanomagnetite (Figure 3C).

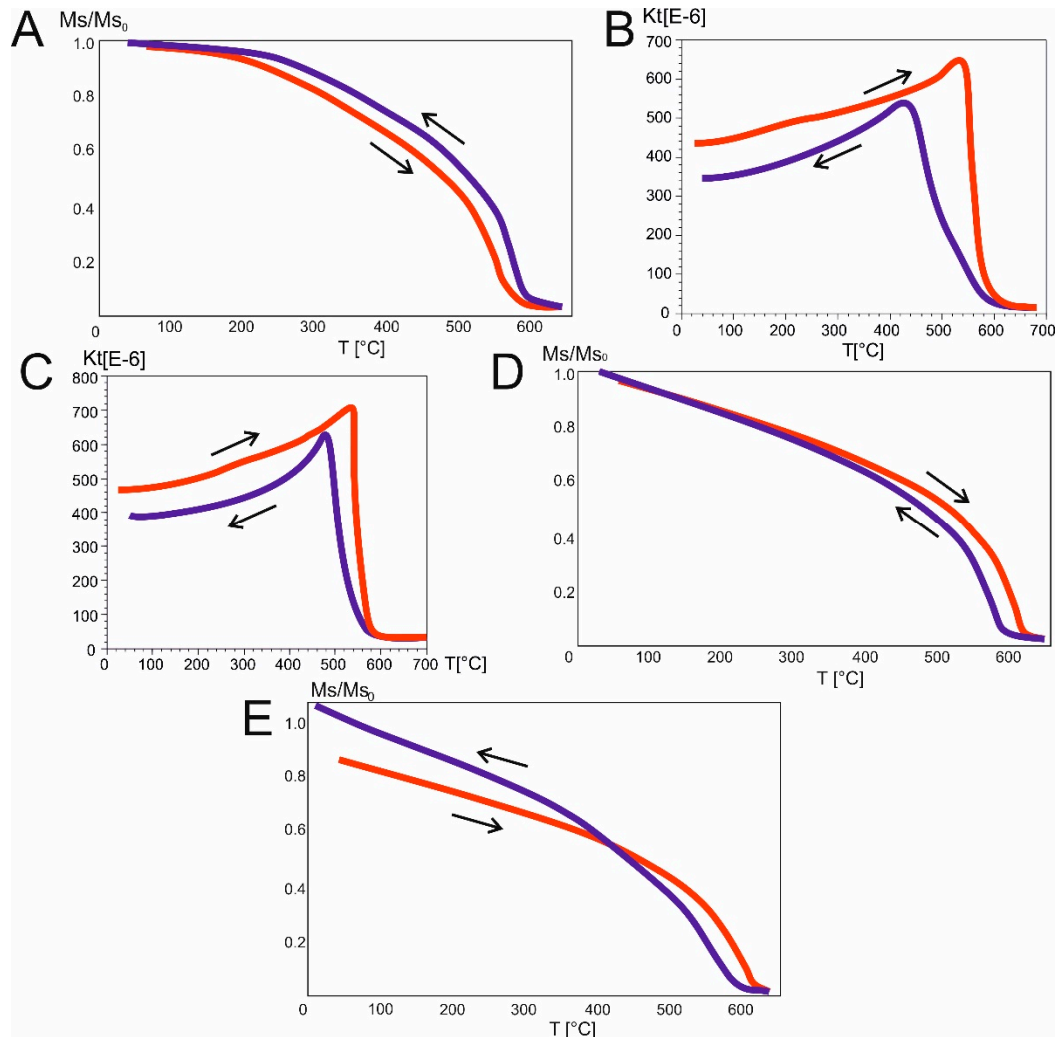


Figure 3. Rock magnetic properties. (A,D,E)—thermal dependences of saturation magnetization. (A)—sample 130, site *on31*, Onkuchaksky Formation. (D)—sample 432, site *tv3*, Tyvankitsky Formation. (E)—sample 733, location 8, Upper Delkansky Formation. (B,C)—thermal dependences of magnetic susceptibility. (B)—sample 161, site *on39*, Onkuchaksky Formation. (C)—sample 40, site *on10*, Onkuchaksky Formation.

Scanning electron microscopy (SEM) of the Onkuchaksky basalts showed widespread dendritic grains of magnetite and titanomagnetite of primary magmatic origin (Figure 4A), both small (3–10 μm) and large (30–100 μm). In large crystals, fracturing typical of the low-temperature oxidation (maghemitization) occurs in some samples (Figure 4B). In general, magnetite partially undergone to maghemitization is the main carrier of remanence in the Onkuchaksky Formation. It should be emphasized that samples with different types of paleomagnetic record (see the Section 4) do not demonstrate regular differences in magnetic mineralogy.

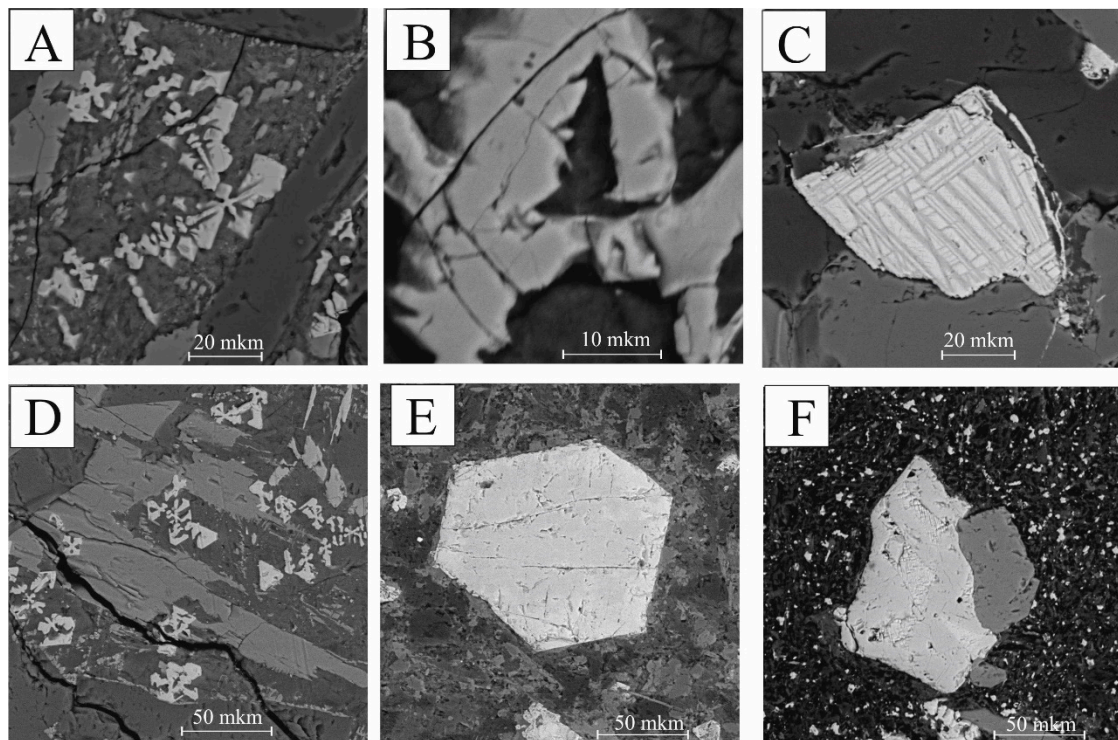


Figure 4. Representative SEM images of the studied samples. (A) Dendrites of titanomagnetite. Sample 140, site *on34*, Onkuchaksky Formation. (B) Titanomagnetite with fracturing typical for low-temperature maghemitization. Sample 164, site *on39*, Onkuchaksky Formation. (C) Titanomagnetite with structures of deuteritic oxidation. Sample 349, site *tv21*, Tyvankitsky Formation. (D) Large dendrites of titanomagnetite. Sample 524, site *s5*, Tyvankitsky Formation. (E) Large titanomagnetite grain with structures of low-temperature oxidation. Sample 228, location 5, Lower Delkansky Formation. (F) Titanomagnetite grain with complex decay structures. Sample 743, location 9, Upper Delkansky Formation.

$M_s(T)$ and $K(T)$ dependences, measured for the samples of the Tyvankitsky Formation, demonstrate the predominance of two magnetic phases with Curie temperatures of about 350–500 °C (titanomagnetite) and 570–590 °C (magnetite). Usually, only one of two these phases occurs in a sample. Most samples demonstrate sustainable magnetic properties after heating-cooling cycles (Figure 3D). Scanning electron microscopy revealed the predominance of titanomagnetite and magnetite grains of variable size. Many large crystals (50–200 μm) are undergone to deuteritic oxidation (Figure 4C). Small (5–10 μm) and medium (20–50 μm) homogenous dendritic grains occur as well (Figure 4D). Also, the detailed rock-magnetic investigation performed on Tyvankitsky samples revealed the presence of single-domain (SD) and pseudo-single domain (PSD) magnetite and titanomagnetite particles [55].

In the rocks of Delkansky Formation, magnetic properties are quite diverse. Two magnetic minerals with Curie temperatures of 570–590 °C (magnetite) and 600–620 °C (partially oxidized magnetite) are the most widely spread (Figure 3E). These phases occur both together and separately. Some curves of magnetic susceptibility demonstrate “tails” up to 675 °C, indicating the presence of hematite as a minor phase. SEM analysis revealed the predominance of large grains of magnetite and titanomagnetite (50–300 μm) with features of low-temperature oxidation (Figure 4E). Occasionally, magnetic grains demonstrate very complicated structures of decay or oxidation, which likely occurred in several stages (Figure 4F). Abundance of secondary alteration probably is responsible for the relatively low quality of paleomagnetic signal in the Delkansky Formation (see the Section 4). However, non-altered small homogenous titanomagnetite crystals are identified as well. Rock-magnetic investigation of samples from the Delkansky Formation confirmed that SD-PSD grains of magnetite or titanomagnetite dominate the magnetic fraction [55].

Thus, microscopic investigation revealed features typical of primary magmatic minerals, e.g., homogenous small grains of magnetite and titanomagnetite, dendritic forms of crystals, structures of the deuteric high-temperature oxidation, which is likely to occur during the lava flow cooling. These are indirect arguments in favor of the primary origin of remanent magnetization. However, severe post-magmatic alteration of magmatic minerals occurs as well, and is probably responsible for the noisy paleomagnetic record in some volcanic units.

4. Paleomagnetism

All paleomagnetic specimens were subjected to the standard stepwise thermal demagnetization. The majority of samples were demagnetized at 560–600 °C, and in a few cases up to 680 °C. The quality of paleomagnetic signal is quite variable; nevertheless, mean paleomagnetic directions were calculated for all formations and units. In general, paleomagnetic directions and virtual geomagnetic poles for all volcanic units are close to those expected for the Permian–Triassic traps of the Siberian platform (e.g., [41]). Some remarkable exceptions are discussed below.

Natural remanent magnetization (NRM) of the Pravoboyarsky tuffs mainly consists of two components (Figure 5A,B). The low-temperature component (LTC) is unblocked at 180–200 °C. In most cases the direction of this component is close to the present-day field direction, therefore we consider LTC to be of viscous origin and do not discuss it further. The high-temperature component (HTC) is isolated at temperatures 180–610 °C and has both normal (13 sites) and reversed (1 site) polarity. Also, in 8 sites the middle-temperature component (MTC) of reversed polarity is isolated at 180–420 °C (Figure 5C). Samples of the picritic dike cutting the studied tuffs demonstrate the HTC of reversed polarity. Since its direction is close to that isolated in tuffs, we consider the reversed MTC and HTC in tuffs to be the result of remagnetization, caused by the emplacement of younger intrusions, widespread in the area of sampling. Furthermore, mean paleomagnetic directions of normal and reversed polarity do not pass the reversal test [56]— $\gamma/\gamma_{cr} = 14.1^\circ/5.8^\circ$, and hence can hardly be resulted from the partial self-reversal of the remanence. Thus, we assume that primary remanence of the Pravoboyarsky formation is of normal polarity. This conclusion is consistent with the previous data from key sections of this formation at the Bolshaya Romanikha and Pravaya Boyarka rivers [48] and with the correlation of Pravoboyarsky tuffs with normally magnetized Arydzhangsky Formation [43]. Mean paleomagnetic direction for the Pravoboyarsky Formation (HTC of normal polarity) is calculated on a sample level (Figure 5D, Table 1).

Paleomagnetic signal in the Onkuchaksky Formation is quite complex and multi-component. The full NRM vector contains up to 3 components (Figure 5E–G). The LTC is demagnetized at 20–240 °C and probably is of viscous nature. The MTC of reversed polarity is usually isolated in the temperature range of 240–540 °C. Finally, the HTC is destroyed at 540–590 °C and demonstrates both normal and reversed polarity in different sites. Similar components were identified after the AF-demagnetization of representative sister specimens with various component composition. The directions of components of normal (N-component) and reversed (R-component) polarities are nearly antipodal ($\gamma/\gamma_{cr} = 8.7^\circ/7.8^\circ$) (Figure 5H). The most stable N-component can be confidently isolated in almost all flows, while the reversed component is identified in many samples from 90% of lava flows, though occurrence of this component is irregular through the lava pile. Finally, 4 flows (two of them are successive) from the middle part of section demonstrate the most stable component of reversed polarity, and in 5 more flows both N- and R-components represent the HTC in different specimens. This component ensemble can be explained by two reasons: (1) partial self-reversal of remanence; and (2) later remagnetization.

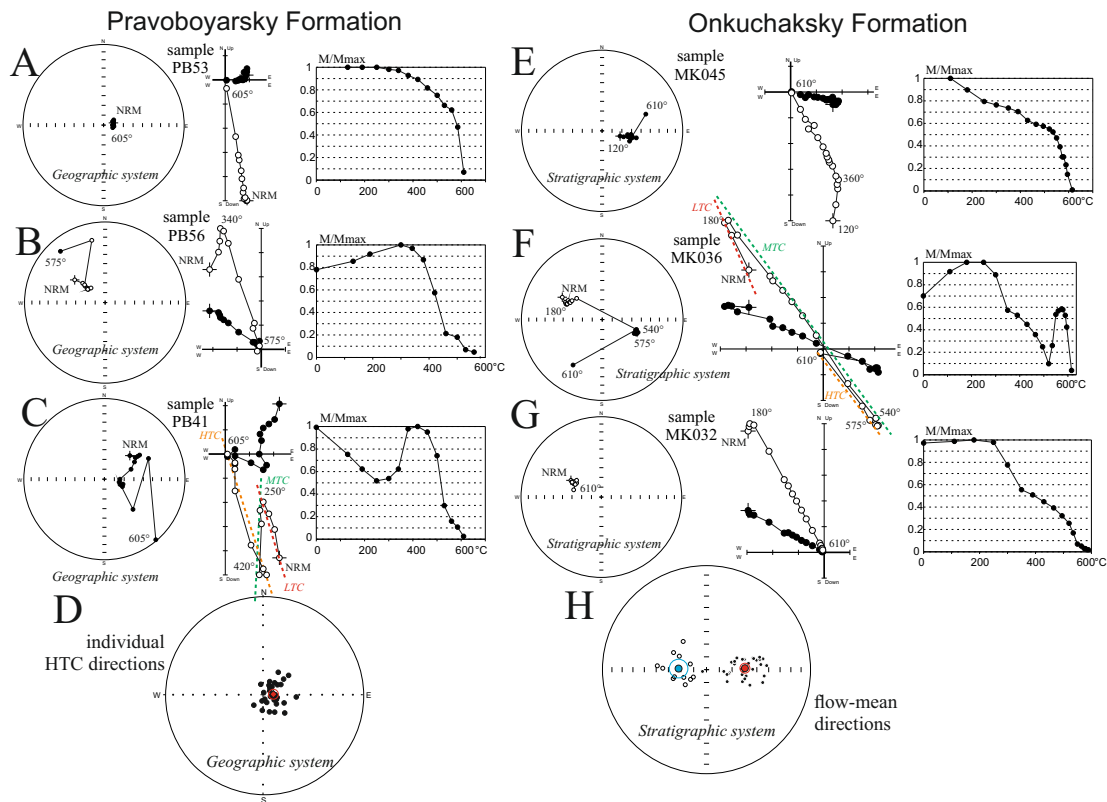


Figure 5. Results of the thermal demagnetization of the Pravoboyarsky and Onkuchaksky formations. (A–C) Representative stereoplots, Zijderveld plots and demagnetization paths for the Pravoboyarsky Formation. (A)—sample PB53, site *pb12*. (B)—sample PB56, site *pb13*. (C)—sample PB41, site *pb10*. (D)—paleomagnetic directions of individual samples for the Pravoboyarsky (geographic coordinate system). (E–G) Representative stereoplots, Zijderveld plots and demagnetization paths for the Onkuchaksky Formation. (E)—sample 45, site *on11*. (F)—sample 36, site *on9*. (G)—sample 32, site *on8*. (H)—site-mean paleomagnetic directions for the Onkuchaksky Formation (stratigraphic coordinate system). Closed (open) circles indicate lower (upper) hemisphere.

Table 1. Paleomagnetic directions and poles of Maymecha River traps.

Site/Flow	N	Dg	Ig	Kg	a95g	Ds	Is	Ks	a95s
Pravoboyarsky Formation (sample-level mean):									
	29	95.6	81.6	45.8	4.0	-	-	-	-
Mean pole: Slat = 70.7°, Slong = 101.2°, Plat = 63.7°, Plong = 140.7°, A95 = 7.6°, paleolatitude = 73.5°									
Picritic dyke, cutting Pravoboyarsky tuffs:									
pb8	4	282.5	-66.6	23.1	19.5	-	-	-	-
Onkuchaksky Formation (high-temperature component):									
on1 (the bottom)	4	107.0	60.5	63.0	11.7	79.2	67.6	63.3	11.6
on2	4	96.8	53.8	145.5	7.6	75.4	59.1	145.6	7.6
on3	5	96.9	59.8	84.7	8.4	69.4	64.4	84.6	8.4
on4	6	107.6	51.5	153.7	5.4	88.9	59.7	153.0	5.4
on5	3	92.0	38.7	40.9	19.5	79.5	43.9	40.9	19.5
on6	3	279.6	-57.2	20.3	28.1	255.0	-62.9	20.3	28.1
on8(N)	2	115.7	51.5	-	-	98.4	61.6	-	-
on8(R)	2	286.3	-65.0	-	-	251.2	-71.2	-	-
on9	4	109.7	53.9	153.5	7.4	89.4	62.4	153.6	7.4
on10	3	103.6	51.1	40.1	19.7	84.8	58.3	40.1	19.7
on11	3	105.9	63.1	101.5	12.3	74.1	69.5	101.9	12.3
on12	2	135.3	57.7	-	-	120.5	71.1	-	-
on13	4	122.8	60.7	26.5	18.2	98.5	71.6	26.5	18.2

Table 1. Cont.

Site/Flow	N	Dg	Ig	Kg	a95g	Ds	Is	Ks	a95s
on14	2	125.3	61.1	-	-	101.5	72.4	-	-
on15	2	168.4	74.4	-	-	242.0	86.6	-	-
on16	4	325.1	-46.5	36.4	15.4	320.4	-61.2	36.4	15.4
on17	3	313.3	-63.9	30.5	22.7	289.2	-76.6	30.5	22.7
on18	5	120.6	41.8	22.8	16.4	109.9	53.3	22.8	16.4
on19	3	127.4	61.6	4.9	63.2	103.7	73.4	4.9	63.2
on20	3	122.4	48.5	59.3	16.1	108.8	60.0	59.6	16.1
on21	3	287.4	-46.9	44.7	18.7	271.9	-55.4	44.5	18.7
on22	4	273.3	-67.4	7.9	35.0	234.7	-69.6	7.9	35.0
on23	4	287.4	-42.0	91.6	9.7	274.5	-50.8	92.1	9.6
on24	4	112.1	33.6	8.3	33.9	103.1	43.7	8.3	33.9
on25	4	114.7	48.2	40.0	14.7	99.5	58.2	40.2	14.7
on26	4	295.1	-71.8	83.5	10.1	240.8	-78.2	83.6	10.1
on27	4	97.7	39.8	21.7	20.2	84.9	46.4	21.7	20.2
on28	6	118.2	48.0	44.1	10.2	103.8	58.8	44.3	10.2
on29	3	94.5	43.8	55.4	16.7	79.6	49.4	55.3	16.7
on30	4	106.4	34.6	12.9	26.6	96.5	43.4	12.9	26.6
on31	3	308.9	-48.1	71.4	14.7	297.4	-60.8	71.7	14.7
on32	4	93.0	47.0	17.2	22.8	76.3	52.0	17.2	22.8
on33	3	111.1	51.6	109.4	11.8	92.9	60.6	108.8	11.9
on34	4	104.9	45.4	103.1	9.1	89.9	53.3	103.5	9.1
on35(N)	2	98.7	42.0	-	-	79.4	46.6	-	-
on35(R)	2	303.0	-69.3	-	-	238.5	-75.4	-	-
on36	5	108.4	49.8	80.7	8.6	82.7	56.8	80.8	8.6
on37(N)	2	96.6	42.5	-	-	77.1	46.4	-	-
on37(R)	2	292.2	-57.3	-	-	257.5	-64.2	-	-
on38	4	107.4	49.7	15.3	24.3	81.8	56.4	15.3	24.3
on39	4	100.1	46.9	19.6	21.3	77.1	51.5	19.6	21.3
on40	3	317.1	-50.4	44.4	18.7	296.4	-66.2	44.5	18.7
on41	3	106.0	55.2	29.1	23.3	74.4	60.5	29.0	23.3
on42	4	101.6	35.1	6.1	40.8	86.4	41.5	6.1	40.8
on43	4	113.7	60.3	75.0	10.7	74.2	67.0	75.0	10.7
on44 (the top)	3	137.5	62.1	6.3	54.1	96.7	76.3	6.3	54.1
Mean (N polarity):	34	109.1	51.4	42.4	3.8	88.3	59.6	40.1	3.9
Mean (R polarity):	12	298.4	-58.1	36.4	7.3	272.2	-68.1	37.0	7.2
Mean MTC (R):	(42)	313.4	-57.8	14.0	6.1	293.5	-71.3	14.4	6.0
Mean pole (HTC N): Slat = 70.8°, Slong = 101.0°, Plat = 38.3°, Plong = 176.8°, A95 = 5.1°, paleolatitude = 40.4°									
Tyvankitsky Formation:									
<i>Location 4:</i>									
s1	4	288.5	-67.0	69.5	11.1	-	-	-	-
s3	3	301.1	-27.9	36.5	20.7	-	-	-	-
s5	6	284.5	-52.0	92.5	7.0	-	-	-	-
s6	6	271.0	-57.7	87.5	7.2	-	-	-	-
s10	5	257.1	-67.4	39.0	12.4	-	-	-	-
<i>Location 5:</i>									
tv33 (the top)	3	264.6	-65.0	159.3	9.8	216.7	-68.7	159.3	9.8
tv32	4	289.4	-58.5	129.6	8.1	255.8	-72.5	129.6	8.1
tv31	4	296.5	-56.9	74.7	10.7	269.7	-73.2	74.7	10.7
tv26	5	93.2	50.2	19.6	17.7	67.6	60.4	19.6	17.7
tv25	3	298.9	-60.5	162.5	9.7	228.7	-55.1	162.5	9.7
tv24	3	236.3	-46.0	29.3	23.2	217.3	-17.7	29.3	23.2
tv23	4	277.9	-49.3	136.2	7.9	237.0	-39.7	136.2	7.9
tv22	6	313.6	-49.3	16.1	17.2	253.1	-60.5	16.1	17.2
tv21	3	259.2	-52.0	36.5	20.7	225.5	-32.0	36.5	20.7
int1	13	283.4	-53.5	37.1	6.9	243.4	-67.0	18.9	9.8
tv20	4	285.2	-51.7	79.0	10.4	257.5	-73.0	79.0	10.4
tv19	3	277.5	-53.6	75.4	14.3	241.1	-71.8	75.4	14.3
tv18	4	305.1	-60.0	52.5	12.8	301.2	-85.0	52.5	12.8
tv16	3	281.2	-55.0	41.9	19.3	235.9	-64.5	24.6	25.4
tv13	4	271.6	-60.7	64.8	11.5	215.5	-74.0	64.8	11.5
tv12	3	287.6	-61.0	244.5	7.9	233.2	-80.8	244.5	7.9
tv11	3	294.3	-62.1	165.9	9.6	239.8	-84.1	165.9	9.6
tv10	4	289.0	-64.2	87.1	9.9	214.9	-82.7	87.1	9.9
tv9	3	291.8	-59.7	25.6	24.9	248.5	-81.6	25.6	24.9

Table 1. Cont.

Site/Flow	N	Dg	Ig	Kg	a95g	Ds	Is	Ks	a95s
tv8	4	294.6	−60.7	83.7	10.1	250.3	−83.3	83.7	10.1
tv7	4	256.2	−54.3	60.6	11.9	215.8	−63.5	60.6	11.9
tv6	3	297.0	−58.6	93.8	12.8	268.8	−82.3	93.8	12.8
tv5	4	269.0	−60.7	64.8	11.5	213.1	−72.9	64.8	11.5
tv4	3	277.9	−51.1	44.5	18.7	246.4	−70.1	45.0	18.6
tv3	4	302.7	−55.6	74.7	10.7	295.1	−80.4	74.7	10.7
tv2	4	294.5	−58.0	68.3	11.2	262.9	−81.2	68.3	11.2
tv1 (bottom)	4	284.3	−58.4	57.7	12.2	238.6	−77.9	57.7	12.2
Mean (R polarity):	31	283.5	−57.6	4602	3.9	247.5	−69.3	16.8	6.5
Mean pole: Slat = 70.8°, Slong = 101.0°, Plat = 56.0°, Plong = 186.4°, A95 = 10.2°, paleolatitude = 52.9°									
Lower Delkansky Formation:									
Location 6 (N)	(4)	54.9	70.1	120.7	8.4	127.3	78.5	121.1	8.4
Location 6 (R)	(15)	340.0	−69.5	22.1	8.3	358.9	−52.1	22.1	8.3
Location 5 (top) *	(51)	265.5	−64.0	8.8	7.2	162.9	−79.8	7.8	7.7
dl42	5	281.5	−62.7	131.3	6.7	240.1	−75.5	97.2	7.8
dl41	3	242.5	−68.0	56.2	16.6	197.0	−63.8	56.2	16.6
dl40	3	229.7	−73.1	39.0	20.0	182.0	−63.8	38.7	20.1
dl38	4	275.6	−43.2	34.4	15.9	256.5	−54.9	34.4	15.9
dl37	4	344.6	−51.0	100.7	9.2	3.5	−68.0	100.7	9.2
dl35 (bottom)	4	218.8	−64.3	50.9	13.0	188.0	−54.7	50.9	13.0
Mean:	8	277.6	−68.5	13.8	15.4	227.0	−79.8	8.9	19.7
Mean pole: Slat = 70.8°, Slong = 101.0°, Plat = 74.7°, Plong = 170.7°, A95 = 36.8°, paleolatitude = 70.2°									
* nonsegmented lavas on the top of Location 5									
Upper Delkansky Formation (sample-level mean):									
Lower part (HTC N)	(21)	68.2	72.3	12.3	9.5	-	-	-	-
Mean pole: Slat = 70.8°, Slong = 100.8°, Plat = 59.5°, Plong = 188.8°, A95 = 15.8°, paleolatitude = 57.5°									
Upper part (HTC R)	(15)	263.3	−53.0	8.4	14.0	228.7	−66.1	6.6	16.1
Mean pole: Slat = 70.8°, Slong = 100.8°, Plat = 58.3°, Plong = 209.4°, A95 = 23.8°, paleolatitude = 48.5°									
Maymechinsky Formation:									
mm1	11	206.5	−78.1	25.1	9.3	214.2	−62.7	25.1	9.3
mm2	10	219.3	−73.4	25.8	9.7	218.8	−57.6	25.8	9.7
mm3	8	258.7	−50.1	11.7	16.9	300.3	−81.5	11.7	16.9
mm4	21	242.8	−54.7	12.2	9.5	222.3	−68.9	8.5	11.6
Mean:	4	240.6	−65.2	24.4	19.0	230.4	−69.3	32.2	16.4
Mean pole: Slat = 70.9°, Slong = 100.7°, Plat = 61.6°, Plong = 203.1°, A95 = 25.8°, paleolatitude = 52.9°									
Samoedsky Formation (Norilsk Region):									
Sm1 (the top)	3	297.8	−75.9	95.5	12.7	-	-	-	-
Sm2	3	287.1	−76.2	78.9	14.0	-	-	-	-
Sm4	6	301.7	−79.3	69.3	8.1	-	-	-	-
Sm6	8	169.5	37.4	36.5	9.3	-	-	-	-
Sm7	5	237.6	84.8	15.6	20.0	-	-	-	-
Sm9 (the bottom)	8	346.8	67.0	96.9	5.7	-	-	-	-

Results of the paleomagnetic investigation. Dg, Ig—declination, inclination in geographic coordinate system; Ds, Is—declination, inclination after tilt correction; K, α_{95} —Fisher statistic parameters [54].

Considering the case of remagnetization, since the HTC of normal polarity is present in almost all flows, it is likely to be of primary magmatic origin. As to the R-component, its irregular occurrence points out that it can be resulted from the selective chemical remagnetization during the later magmatic events. However, mechanism of this remagnetization is still unclear, because samples with different sets of remanence components demonstrate, in general, similar magnetic mineralogy (see the Section 3). As to the samples with the high-temperature R-component, in this case they are to be fully remagnetized. The version of primary nature of R-component seems us to be unrealistic, because in most flows where it is isolated as HTC, this component occurs along with HTC of normal polarity in some samples.

As for the partial self-reversal of the remanent magnetization, it has been reported in many regions of the Siberian Traps [57–59]. Composition of magnetic minerals, identified with rock-magnetic and microprobe analysis, allows us to suggest the spinodal decay of titanomagnetite [60] or interaction in titanomagnetite-maghemite associations [59,61] as possible mechanisms of self-reversal. In all those cases, the most stable N-component corresponds to the geomagnetic polarity in time of the lava flow eruption.

Thus, we can assume that HTC of normal polarity in the Onkuchaksky basalts is of primary magmatic origin. However, the problem of self-reversal in the Siberian Traps rocks requires the special investigation, because similar features of paleomagnetic record are widespread [33,62,63]. Mean paleomagnetic directions of N-component for 34 lava flows were calculated (Table 1; Figure 5H).

Lava flows of the Tyvankitsky Formation usually show a clear paleomagnetic record at profile 5 (Figure 2A), and a signal of variable quality—at profile 4. Besides the low-temperature viscous component, the only stable component is isolated mainly in the temperature range 240–600 °C (Figure 6A). This component is of reversed polarity, with the exception of flow 26 in the profile 5, where it demonstrates positive inclinations. In a couple of adjacent flows, directions of the HTC are significantly different from those expected for the Permian–Triassic Traps [41] and have anomalously low inclinations. This group of flows probably marks the geomagnetic excursion, though cases of unrecognized block dislocations or contribution of overprinting components cannot be completely excluded. The mean direction for the Tyvankitsky Formation has been calculated using site-mean directions for 31 flows (Figure 6E).

Samples of the Delkansky Formation volcanics usually demonstrate 2-component paleomagnetic signal of variable quality. The LTC is isolated in many samples below 180 °C and probably is of viscous origin. The HTC is unblocked in the temperature range 180–585 °C and decays to origin at orthogonal plots (Figure 6B). In the Lower Delkansky unit this component usually has reversed polarity, and its directions are widely scattered (Figure 6F). Only in location 6 did some samples, uppermost in a section, yielded the HTC of normal polarity. For the calculation of the mean paleomagnetic direction for the Lower Delkansky Formation, we used 6 flow-mean directions, the mean direction for the inseparable interval (profile 5), and the mean direction for the location 6 (Table 1).

In the Upper Delkansky, unit the HTC demonstrates normal polarity in lowermost flows, corresponding to location 8 (Figure 6G), while in the uppermost part of formation interchange of normal and reversed intervals is observed. Paleomagnetic directions of both reversed and normal polarity are scattered. Probably, lavas of the uppermost interval of unstable polarity have been partially remagnetized by the overlying Maymechinsky Formation; however, we cannot exclude the possibility that this interval corresponds to the transitional unstable geomagnetic field. The mean direction for the Upper Delkansky Formation (N-component) was calculated on a sample level (Table 1).

Thus, the Lower Delkansky unit was erupted during the reversed interval, while the formation of Upper Delkansky unit corresponds to the chron of normal polarity. It should be noted that the uppermost samples of normal polarity in the Lower Delkansky unit (location 6) may indicate the transition to the Upper Delkansky interval of normal polarity.

Ultramafic rocks of the Maymechinsky Formation usually demonstrate a clear paleomagnetic signal. Almost all samples contain the only component of NRM (20–590 °C) of reversed polarity (Figure 6C). It should be noted that the value of NRM in Maymechinsky lavas is three orders higher than in other formations (with the exception of few samples from Pravoboyarsky tuffs). Mean paleomagnetic direction was calculated using four site-mean directions (Figure 6H; Table 1).

In basalts of the Samoedsky Formation, NRM is a sum of low-temperature and high-temperature components (Figure 6D), which are isolated in the temperature ranges 20–180 °C and 180–610 °C, respectively. Lower part of the sampled interval is characterized by the normal polarity of HTC, while the upper part demonstrates reversed polarity (Figure 6I; Table 1). It's worth noting that normal polarity directions differ from the expected Permian–Triassic geomagnetic field direction. Since that, we suggest that these directions may represent a record of transitional geomagnetic field. However,

it can also be caused by unconsidered tilt correction due to poor exposure. Thus, our data confirms the suggestion about the presence of the reversed polarity interval in the uppermost Samoedsky Formation [31,64].

Thus, we obtained the paleomagnetic record for all stratigraphic units for the Maymecha river valley and completed the magnetostratigraphic section of the Norilsk regions. Arguments in favor of the primary nature of the remanence in the Maymecha extrusive rocks are as follows:

1. Proximity of the most of obtained paleomagnetic directions to those expected for the P-T of the Siberian Traps [41].
2. Positive “baked contact test”: Pravoboyarsky tuffs in the contact zone of the picritic dike are partially remagnetized, but the primary component of normal polarity is still preserved.
3. Presence of the primary magmatic magnetites and titanomagnetites, often with the structures of the deuteric oxidation.
4. Reliable determinations of the paleointensity for the Tyvankitsky and Delkansky formations [55], pointing to the thermoremanent origin of NRM.

As to the Samoedsky Formation, the positive regional fold test for the Kharaelakh trough presented in [41] for the Morongovsky Formation, confirms the pre-folding age of the remanence acquisition.

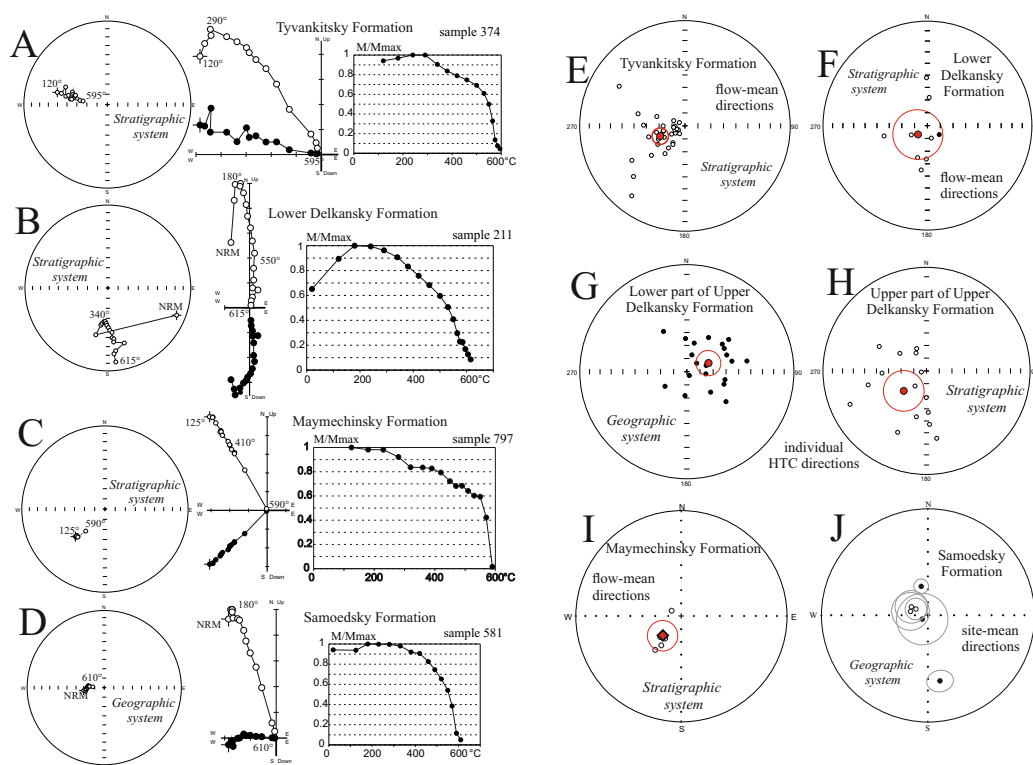


Figure 6. Results of the thermal demagnetization of the Tyvankitsky, Delkansky, Maymechinsky, and Samoedsky formations. (A–D) Representative stereoplots, Zijderveld plots and demagnetization paths. (A)—sample 374, site *tv18*, Tyvankitsky formation. (B)—sample 211, location 5, Lower Delkansky Formation. (C)—sample 797, site *mm5*, Maymechinsky Formation. (D)—sample 581, site *sm4*, Samoedsky Formation. E–J. Distribution of paleomagnetic directions. (E)—Tyvankitsky Formation, site-mean directions, stratigraphic coordinate system. (F)—Lower Delkansky Formation, site-mean directions, stratigraphic coordinate system. (G)—lower part of the Upper Delkansky Formation, geographic coordinate system. (H)—upper part of the Upper Delkansky Formation, geographic coordinate system. (I)—Maymechinsky Formation, site-mean directions, stratigraphic coordinate system. (J)—Samoedsky Formation, site-mean directions geographic coordinate system. Closed (open) circles indicate lower (upper) hemisphere.

5. Discussion

Despite the variable quality of paleomagnetic record, we calculated mean virtual geomagnetic poles (VGP) for all volcanic formations (Table 1). As seen in Figure 7, almost all VGPs after tilt correction are significantly different from the paleomagnetic pole NMK (Norilsk-Maymecha-Kotuy) for the Permian–Triassic Traps of the Siberian platform [41]. This difference can be caused by several reasons, alone or together: (1) insufficient averaging of secular geomagnetic variations; (2) relatively low accuracy and precision of some of obtained VGP; (3) incorrectly accounted tilting; or (4) possibly younger age of the essential part of the Maymecha volcanic section comparing with the main volume of the Siberian Traps (see below). We note that VGPs of the upper part of the Maymecha section (Tyvankitsky, Delkansky, Maymechinsky formations) are virtually close to the pole of the youngest differentiated intrusions from the Nizhnyaya Tunguska river valley reported by Latyshev et al. (2018) [42]. In any case, we consider that quality of VGPs for the Maymecha volcanic formations is too low to use them for any quantitative comparison.

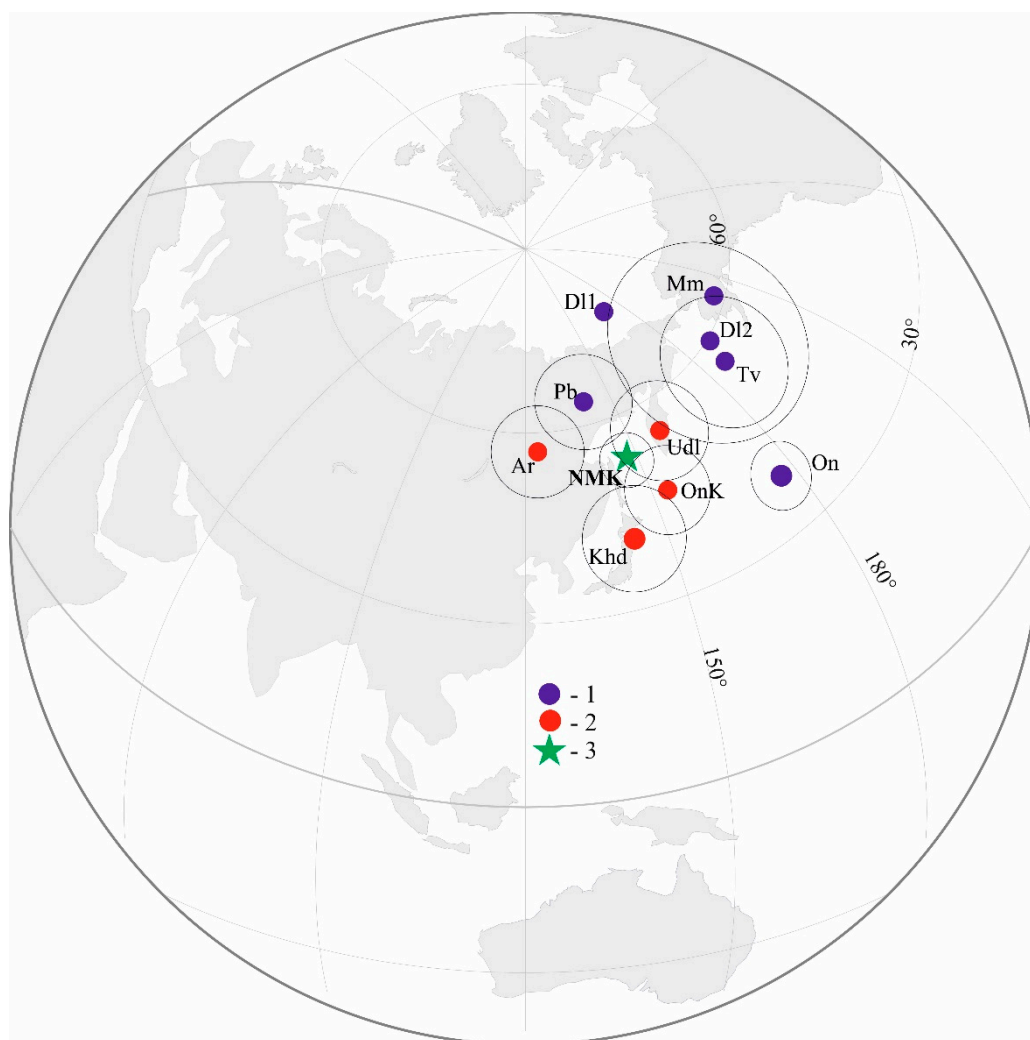


Figure 7. Position of mean virtual geomagnetic poles for the studied formations (stratigraphic coordinate system). (1)—this study: Pb—Pravoboyarsky; On—Onkuchaksky; Tv—Tyvankitsky; D11—Lower Delkansky; D12—Upper Delkansky; Mm—Maymechinsky Formation. Confidence circles for D11 and Mm poles are not shown. (2)—previously published poles: Ar—Arydzhangsky Formation [33]; On—Onkuchaksky Formation in the Kotuy river valley [33]; Udl—Ust-Delkan dike complex [65]. (3)—paleomagnetic pole NMK [41].

On the basis of new paleomagnetic results, we can adjust the correlation of volcanic sections of the Maymecha and Kotuy river valleys. Since the sampled sections of the Pravoboyarsky Formation are magnetized in normal polarity, they are likely coeval to the Arydzhangsky Formation from the Kotuy lava sequence. This suggestion is consistent with the paleontological data on the P-T boundary position within the Pravoboyarsky and Arydzhangsky formations [45,46] and the correlation scheme given in [43]. In this case, the same interval of normal polarity comprises the lowermost part of the Onkuchaksky Formation in the Kotuy river valley (“Truba” gorge in [33]) and the whole section of the Onkuchaksky Formation in the Maymecha river valley (profile 3 in Figure 2A). The overlying interval of the reversed polarity is represented by the upper part of the Onkuchaksky Formation in the valley of Kotuy and by the Tyvankitsky and Lower Delkansky formations in Maymecha district. The younger intervals of the normal and reversed polarity are recorded only in the valley of Maymecha within the Upper Delkansky and Maymechinsky formations, respectively. Dikes of the Ust-Delkan complex cutting the whole Maymecha volcanic sequence and showing the reversed polarity [65] probably belong to the latter interval as well. Finally, according to this scheme, the Khardakhsky tuffs contain the record of the most ancient interval of reversed polarity and represent the earliest manifestation of volcanic activity in the Maymecha-Kotuy region (Figure 8).

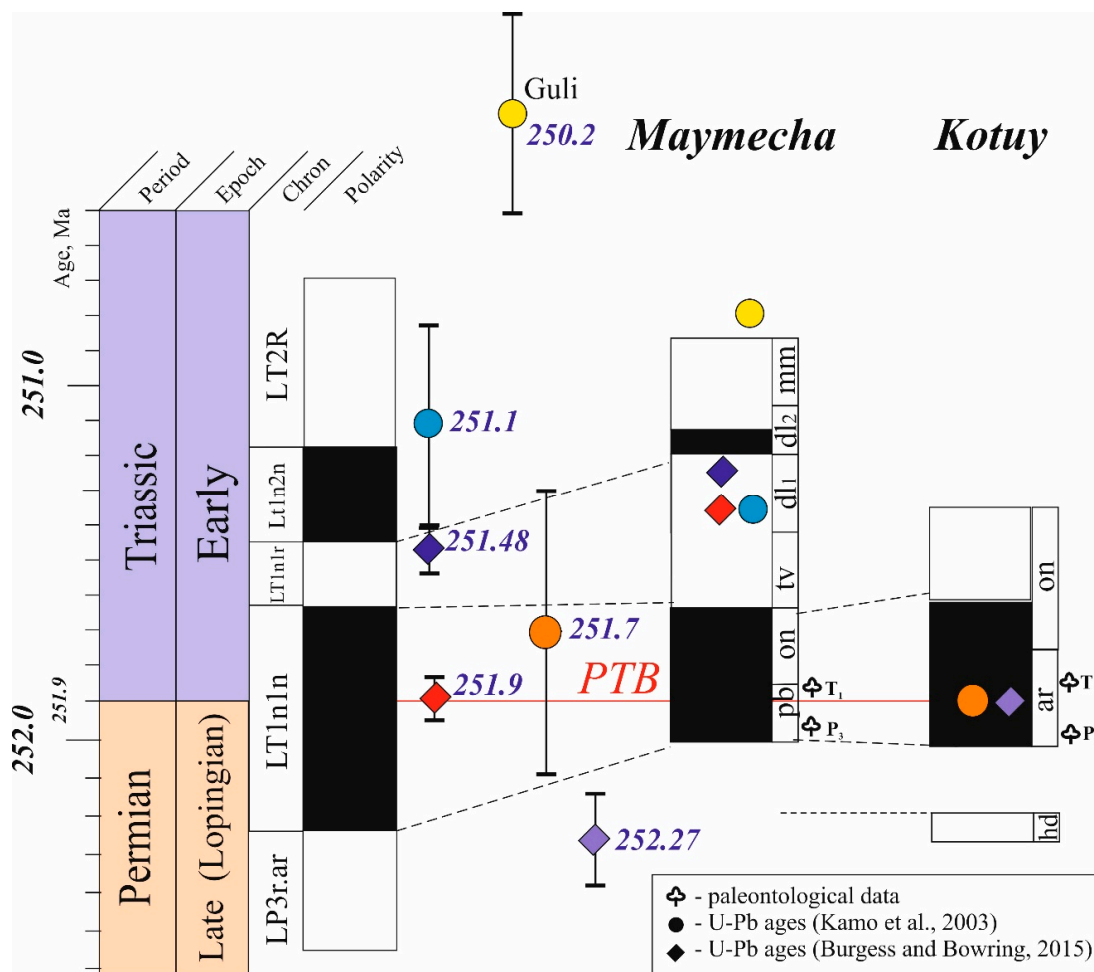


Figure 8. Magnetic stratigraphy and correlation of the Maymecha and Kotuy volcanic sections. Abbreviations of volcanic formations: pb—Pravoboyarsky; on—Onkuchaksky; tv—Tyvankitsky; dl—Delkansky; mm—Maymechinsky; hd—Khardakhsky; ar—Arydzhangsky. Nomenclature of magnetic chrons is given after [66]; their boundaries—after [67,68]. Position of PTB is shown after [47].

The next task is to reconcile the suggested scheme with the available geochronological data. As was shown above, two groups of high-precise U-Pb ages were obtained for the Maymecha-Kotuy magmatic rocks: by Kamo et al. (2003) [15] and by Burgess and Bowring (2015) [29]. These ages, whilst close, are not completely consistent to each other. The possible versions of correlation are considered further.

If we take as a basis U-Pb ages from [15], then the age of Arydzhangsky Formation is 251.7 ± 0.4 Ma, being slightly younger than PTB after [47], but overlapping this boundary within the confidence intervals. This interpretation is completely consistent with the paleomagnetic and paleontological data. Then, the interval of normal polarity recorded in the Arydzhangsky and Pravoboyarsky formation, corresponds to subchron LT1n1n (following the nomenclature of [66,67]), which contains the Permian–Triassic boundary in its lower part. Furthermore, the Tyvankitsky and Lower Delkansky formations in Maymecha district, as well as the upper part of Onkuchaksky Formation in Kotuy area, correspond to subchron LT1n1r. Lower Delkansky Formation is dated by Kamo et al. (2003) [15] at 251.1 ± 0.3 Ma, that is a little younger than the end of this subchron attributed at 251.444 Ma [67]; however, considering the confidence interval, this dating almost coincides with the chron boundary. We emphasize that in this case only the Khardakhsky Formation is definitely older than the Permian–Triassic boundary and the onset of extinction (Figure 8).

If we accept U-Pb ages of Burgess and Bowring (2015) [29], then the dated lava flow from the Arydzhangsky Formation (252.27 ± 0.15 Ma) is older the onset of extinction and Permian–Triassic boundary. The latter contradicts the paleontological data [46], nevertheless, even in this case the interval of normal polarity comprising the Arydzhangsky Formation corresponds to the subchron LT1n1n, if accepting its boundaries from [67]. However, Burgess and Bowring (2015) [29] placed this interval below the PTB and attributed it, apparently, to subchron LP3r.an [67]. Furthermore, the Delkansky Formation is dated by these authors as 251.901 ± 0.089 Ma and 251.483 ± 0.11 Ma. The former of these ages strikingly coincides with the PTB after [47], while the latter is ~400 kyr younger. Burgess and Bowring (2015) [29] argued that these ages enclose the gap in eruptions during the subchron LT1n1n. However, we do not know any evidence of so prolonged gap within the Delkansky Formation. Moreover, the older of these ages contradicts (1) findings of Lower Triassic phyllopoths in the Pravoboyarsky Formation [45] and (2) the position of the Permian–Triassic boundary within the interval of normal polarity [67,69]. Thus, we consider the age of 251.901 ± 0.089 Ma to be less reliable than others and do not take it into account further. Possibly, zircons from felsic tuffs, which yielded this age, represent antecrysts of earlier magma pulses in deep staging chambers [70,71]. In this case, the reversed polarity interval comprising the Tyvankitsky and Lower Delkansky formations should be Lower Triassic and referred to as subchron LT1n1r.

The next step is to correlate the volcanic sections of Norilsk and Maymecha-Kotuy regions. The previous paleomagnetic investigation showed that the Norilsk volcanic sequence comprises (from bottom to top): (1) reversely magnetized Ivakinsky Formation; (2) thick “transitional” zone, including intervals of the geomagnetic reversal and the following excursion (from Syverminsky to the middle part of Nadezhdinsky formations); (3) interval of stable geomagnetic field of normal polarity (from the uppermost Nadezhdinsky to Kumginsky formations) [31,38–41]. Our new data confirms the presence of the reversed polarity interval in the uppermost Samoedsky Formations, as suggested before by Lind et al. (1994) [64] and Gurevitch et al. (2004) [31]. Paleontological findings point out to the Late Permian age of the Ivakinsky Formation and the Early Triassic age of the Kharaelakhsky Formation [72]. Based on this information, it is generally accepted the PTB is set at the Ivakinsky–Syverminsky boundary (e.g., [20]). An alternate hypothesis was suggested by Burgess and Bowring (2015) [29], who placed the whole Norilsk volcanic section below the PTB based on the correlation with the Maymecha-Kotuy volcanic sequence, which has been considered to be Permian to by these authors. In this scheme, the ore-bearing intrusions of the Norilsk type postdate the volcanic activity and PTB with U-Pb ages of ~251.9–251.6 Ma [29]. However, the recent paleomagnetic investigation has shown that all Norilsk-type intrusions are coeval to the Morongovsky-Mokulaevsky formations [30], as suggested by ([73,74] and

some other authors). Then, taking into account U-Pb ages from [29], the Permian–Triassic boundary has to be set below the Morongovsky-Mokulaevsky formations, but within the same interval of normal polarity according to [67]. Since that, we conventionally place the Permian–Triassic boundary at the base of Morongovsky Formation, as it is the sharp frontier in geochemical features (e.g., [75,76], magnetic stratigraphy [41], and this interpretation is consistent with geochronological and paleontological data. The full data is to be published elsewhere (Latyshev et al., in prep.).

Thus, our data supports the suggestion that volcanic sections of Norilsk and Maymecha-Kotuy are partially overlapped [14,33,43,77]. The chron of reversed polarity LP3r (the latest in Permian) comprises the Ivakinsky (Norilsk) and Khardakhsky (Kotuy) formations (Figures 8 and 9). The most of overlying tuff-lava sequence of Norilsk, as well as the Arydzhangsky, Pravoboyarsky and, in part, Onkuchaksky formations, are referred to as subchron LT1n1n. The next interval LT1n1r includes the uppermost Onkuchaksky Formation in the Kotuy area, Tyvankitsky and Lower Delkanskyy formations in the Maymecha district, and the uppermost Samoedsky Formation in the Norilsk region. Also, intrusions of the Dal'dykan complex, widespread in the Norilsk region, cut the whole volcanic sections, are reversely magnetized [64] and appear to be emplaced within the same interval. However, we note that U-Pb age of the Dal'dykan intrusions (251.376 ± 0.082 Ma) obtained by Burgess and Bowring (2015) [29] is younger than the upper boundary of subchron LT1n1r of 251.444 Ma [67]. As to the Upper Delkanskyy (normal polarity) and Maymechinskyy formations (reversed polarity), they correspond to intervals LT1n2n and LT2R, respectively [66,68].

Thus, the main volume of the volcanic pile of the northern Siberian platform is younger than the PTB. However, the onset of biotic crisis nearly coincides to the boundary of reversed and normal intervals of magnetic polarity in Global Stratotype Section and Point (GSSP) Meishan section [78]. If so, than Ivakinsky subalkaline basalts and Khardakhsky alkaline-ultramafic tuffs immediately preceded the beginning of extinction. Moreover, manifestations of nearly coeval volcanic events in the end of Permian are identified in other regions of the Siberian Traps LIP (Figure 9). In the central part of Tunguska syncline Sidoras (1984), [49] reported the reversed polarity in the lowermost volcanoclastic Tutonchanskyy Formation. However, paleomagnetic data in the cited work were obtained without common up-to-date techniques (full demagnetization, principle component analysis, etc.) and therefore need revision. Furthermore, in the Angara-Taseeva depression we identified the reversed polarity in tuffs of the Korvunchanskyy (or Kapaevskyy in some papers [79]) Formation at the single site near the Badarma river [80]. These tuffs represent the southernmost outcrop of the volcanoclastics within the Siberian platform and are likely to be the oldest in this area. Outside the Siberian platform, the lowermost in the volcanic section of Taymyr subalkaline basalts of Syradasaysky Formation demonstrate the reversed polarity and are correlated with the Ivakinsky Formation [81]. Finally, reversely magnetized volcano-sedimentary sequence of the Kuznetsk basin is attributed to the Upper Permian as well [82].

There is a widespread point of view that initial stage of the Siberian Traps volcanic activity occurred as explosive eruptions that could dramatically affect the environment [17,20,83–85]. However, our results show that pre-extinction explosive events have been either local (Angara-Taseeva depression, Kotuy river valley) or of unclear scale (Tunguska syncline). The most voluminous end-Permian magmatic event is the eruption of Ivakinsky lavas, which occupy the whole Norilsk region and constitute the thick (up to 330 m [26]) monolithic packet of lava flows (Figure 10A). Also, though the Khardakhsky volcanoclastic rocks occur only in a limited area, we believe that the volume of explosive magmatic activity in the Kotuy river area can be underestimated. During the field work in the Kotuy river valley, within the Paleozoic sediments we found volcanic breccia pipes of alkaline-ultramafic rocks with bombs of syenites, alkaline lavas, carbonates, and other rocks (Figure 10B,C). Also, boulders of meimechite-like breccia were found at the towpath of Kotuy (Figure 10D). We note that magmatic rocks of meimechitic and syenitic composition have never been reported in the Kotuy river valley before. However, the timing and volume of related magmatism remain vague.

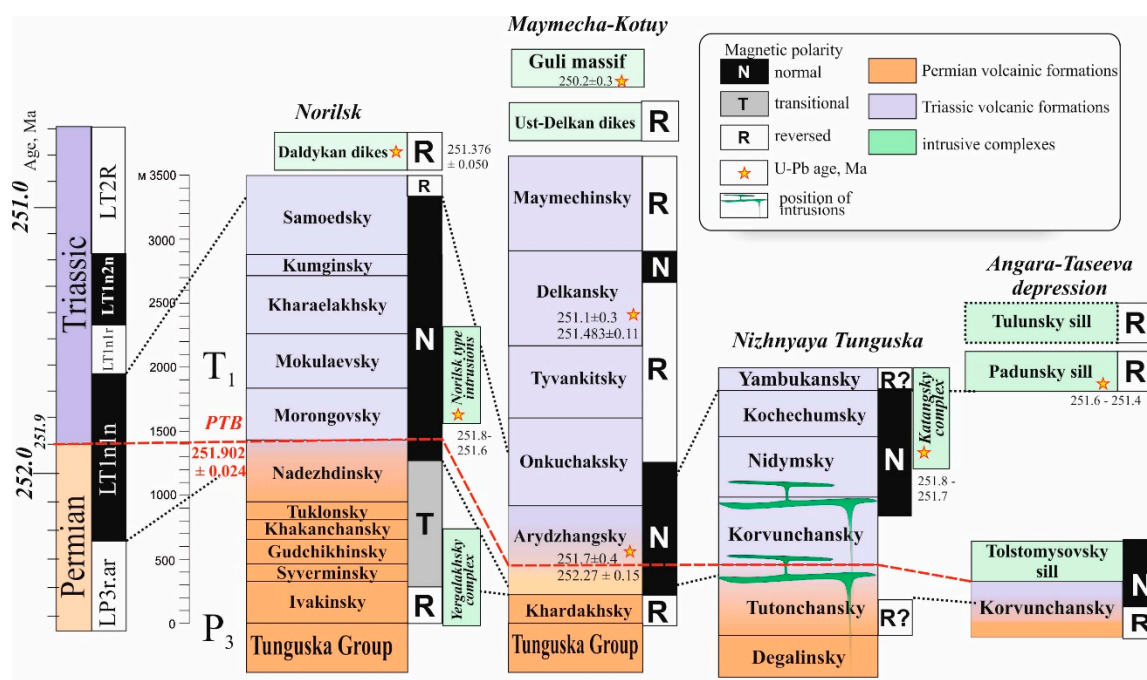


Figure 9. Correlation scheme for regions of the Siberian Traps LIP. After [42], with changes. U-Pb data from [15,29,47]. Magnetic polarity data after ([33,41,42,49,63,64,80] this study). Chrons of Global Polarity Timescale after [66–68].

Many authors consider intrusive bodies of the Siberian LIP as an important agent of environmental changes, due to the contact interaction of large sills and host sedimentary rocks and related volatile release [17,86–88]. The only group of intrusions, which is confidently older than the onset of biotic release [17,86–88]. The only group of intrusions, which is confidently older than the onset of biotic crisis, is the Yergalakhsky complex of trachydolerites (Figure 9). Sills of this complex are widespread in the Norilsk region, are considered to be the intrusive analogues of the Ivakinsky Formation according to geochemical features [26], and some of them have reversed polarity [63,64]. Yergalakhsky sills are located in the coal-bearing sandstones of the Tunguska Group, and in many outcrops intrude the coal beds (Figure 10E,F). Such relationships possibly led to the combustion of coal and released the significant amount of CO₂.

As seen in Figure 9, the main stage of magmatic activity during the Siberian Traps emplacement corresponds to the chron LT1n1n above the PTB. This can be important considering the idea of two stages of the Permian–Triassic biotic crisis [89–91]. The second pulse of mass extinction is attributed to the conodont zone *Isarcicella staeschei*, corresponding to Bed 28 in GSSP section of Meishan [90,92]. This bed is located within the same interval of normal magnetic polarity LT1n1n [78] and is dated at 251.880 ± 0.031 Ma by [47]. Thus, the main stage of volcanic activity in the Siberian platform can overlap the younger pulse of extinction.

Our data points out that the Permian–Triassic volcanic activity in the Maymecha-Kotuy region lasted much longer than in other areas of the Siberian platform. The upper part of the Onkuchaksky Formation (in the Kotuy river valley), as well as the whole Tyvankitsky, Delkansky, and Maymechinsky formations erupted after the cessation of volcanism within the Siberian platform, comprising three magnetic polarity intervals. According to the duration of the corresponding chron presented in [68], the duration of this final stage of volcanic activity can be estimated as ~600 kyr. Taking into account the U-Pb age of baddeleyite from Guli carbonatites of 250.2 ± 0.3 Ma [15], the whole duration of magmatic activity in the Maymecha-Kotuy region was at least about 2 Myr.

Finally, we pay attention that the available timescales of magnetic polarity near the PTB need the further adjustment. For instance, the estimated duration of subchron LT1n1n is widely variable. Szurlies (2012; 2013) [93,94] suggested that this chron lasted about 700 kyr based on cyclostratigraphic

analysis of the Permian–Triassic sediments. In the papers [67,69], its duration is estimated as 608 kyr and 401 kyr, respectively, on the basis of the mathematical modeling. However, most of the U-Pb ages used in two latter papers [47,95,96] are very close to each other and partially overlap within the confidence intervals. Moreover, some of them are older than the PTB age of [47]. Thus, this problem requires an additional investigation.

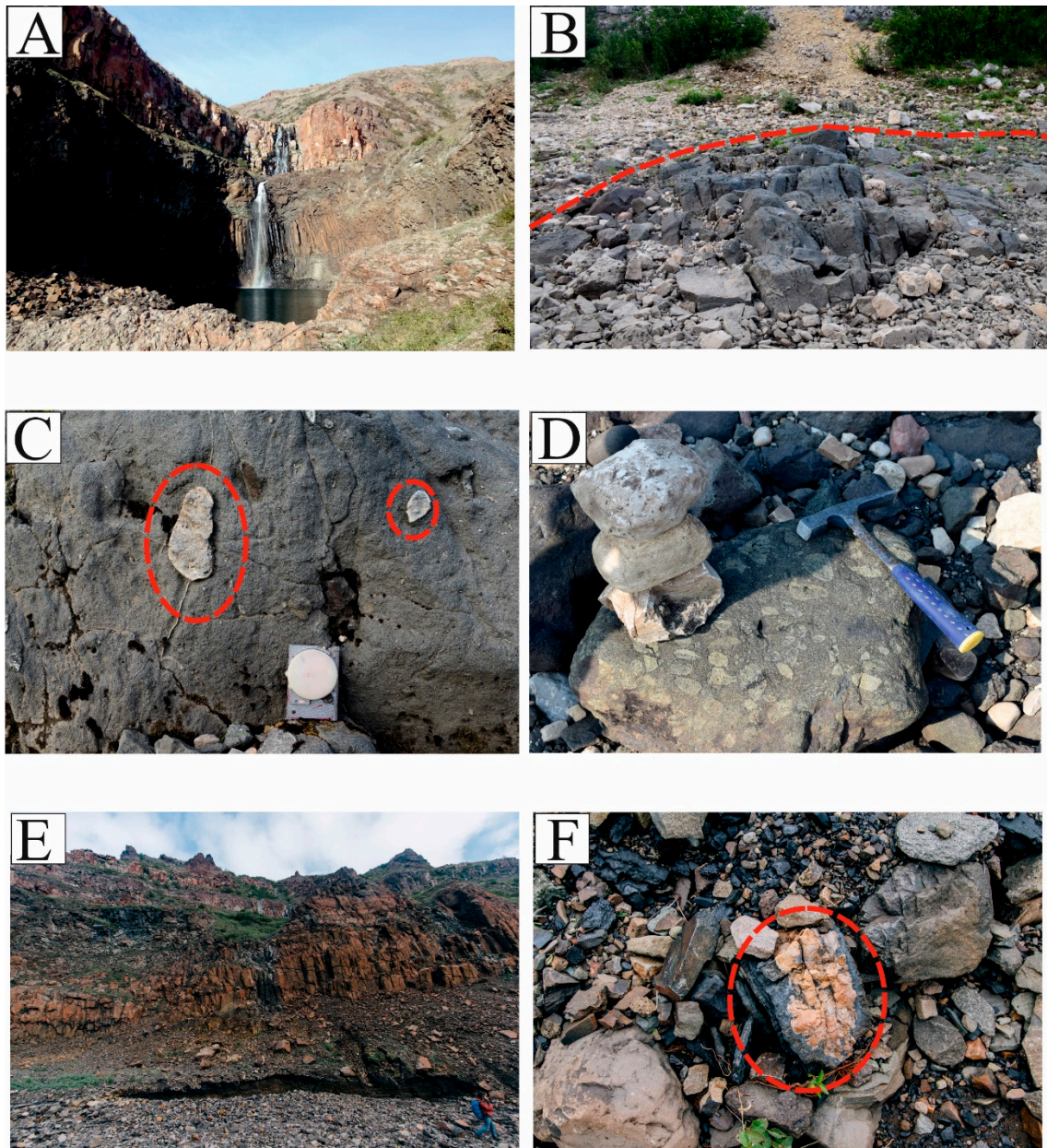


Figure 10. (A) Lava flows in the bottom of Ivakinsky Formation near the town of Talnakh. Thickness of the lowermost flow is about 50 m. (B) An outcrop of the alkaline-ultramafic breccia pipe in the Kotuy river valley. (C) Large clasts of syenites and ultramafic rocks in the volcanic breccia, the Kotuy river. (D) Boulder of olivine-rich breccia with lithic clasts of meimechites, the Kotuy river. (E) Sill of the Yergalakhsky complex intruding coal-bearing sediments of the Tunguska Group, the Norilsk region. (F) Intrusive contact of Yergalakhsky trachydolerites and coals of the Tunguska Group (in a boulder).

6. Conclusions

1. The Permian–Triassic volcanic section of the Maymecha-Kotuy region comprises five intervals of magnetic polarity and corresponds to the most prolonged eruptive activity within the Siberian platform.
2. The major part of the Maymecha-Kotuy volcanic section erupted in the beginning of Early Triassic and postdate came the onset of end-Permian mass extinction, as did the main volume of the Siberian Traps.
3. The initial pulse of volcanic activity in the Maymecha-Kotuy region took place at the end of the Permian period and preceded the biotic crisis. Coeval explosive events are identified in other regions of the Siberian Traps LIP; however, their scale is still unclear.
4. The most voluminous magmatic event of this initial stage occurred in the Norilsk region and corresponds to the emplacement of the thick Ivakinsky lava formation and sills of the Yergalakhsky complex intruding coal-bearing sediments of the Tunguska Group.
5. The total duration of magmatic activity in the Maymecha-Kotuy region can be estimated as ~2 Myr. This lasted after the termination of eruptions in other parts of the Siberian platform.

Author Contributions: All authors performed the field work and paleomagnetic procedures. A.V.L. carried out rock-magnetic investigation, made the interpretation and scheme of correlation and wrote the manuscript. A.M.F. and R.V.V. processed the paleomagnetic data, made figures and edited the text. All authors have read and agreed to the published version of the manuscript.

Funding: This study was supported by Russian Foundation for Basic Research (projects 18-35-20058, 18-05-70094 and 20-05-00573).

Acknowledgments: Authors gratefully thank V.A. Tseltmovich for the SEM and EDS analysis, V.E. Pavlov for the continuous participation in the work and productive discussions, S. Burgess and B. Black for taking part in the field trip in the Maymecha river valley, and P. Ulyakhina and N. Salnaya for the photos provided. We also thank anonymous reviewers for their valuable comments.

Conflicts of Interest: Authors declare no conflict of interest.

References

1. Vogt, P.R. Evidence for global synchronism in mantle plume convection, and possible significance for geology. *Nature* **1972**, *240*, 338–342. [[CrossRef](#)]
2. Courtillot, V. *Evolutionary Catastrophes: The Science of Mass Extinctions*; Cambridge University Press: Cambridge, UK, 1999.
3. Bond, D.P.G.; Wignall, P.B. Large igneous provinces and mass extinctions: An update. In *Volcanism, Impacts and Mass Extinctions: Causes and Effects*; Keller, G., Kerr, A.C., Eds.; Geological Society of America Special Paper: Boulder, CO, USA, 2014; pp. 29–55.
4. Ernst, R.E.; Youbi, N. How Large Igneous Provinces affect global climate, sometimes cause mass extinctions, and represent natural markers in the geological record. *Palaeogeogr. Palaeoclim. Palaeoecol.* **2017**, *478*, 30–52. [[CrossRef](#)]
5. Raup, D.M.; Sepkoski, J.J. Mass extinctions in the marine fossil record. *Science* **1982**, *215*, 1501–1503. [[CrossRef](#)] [[PubMed](#)]
6. Wignall, P.B. Large igneous provinces and mass extinctions. *Earth Sci. Rev.* **2001**, *53*, 1–33. [[CrossRef](#)]
7. Courtillot, V.; Olson, P. Mantle plumes link magnetic superchrons to phanerozoic mass depletion events. *Earth Planet. Sci. Lett.* **2007**, *260*, 495–504. [[CrossRef](#)]
8. Kravchinsky, V.A. Paleozoic large igneous provinces of Northern Eurasia: Correlation with mass extinction events. *Glob. Planet. Chang.* **2012**, *86–87*, 31–36. [[CrossRef](#)]
9. Blackburn, T.J.; Olsen, P.E.; Bowring, S.A.; McLean, N.M.; Kent, D.V.; Puffer, J.; McHone, G.; Rasbury, E.T.; Et-Touhami, M. Zircon U-Pb geochronology links the end-triassic extinction with the central Atlantic magmatic province. *Science* **2013**, *340*, 941–945. [[CrossRef](#)]
10. Masaitis, V.L. Permian and Triassic volcanism of Siberia: Problems of dynamic reconstructions. Notes of the all-Union mineralogical society. *Zap. Vseross. Miner. Obs.* **1983**, *112*, 412–425. (In Russian)

11. Reichow, M.K.; Saunders, A.D.; White, R.V.; Pringle, M.S.; Al'mukhamedov, A.I.; Medvedev, A.I.; Kirda, N.P. 40Ar/39Ar dates from the West Siberian Basin: Siberian flood basalt province doubled. *Science* **2002**, *296*, 1846–1849. [[CrossRef](#)]
12. Ernst, R.E. *Large Igneous Provinces*; Cambridge University Press: Cambridge, UK, 2014; ISBN 9781139025300.
13. Renne, P.R.; Basu, A.R. Rapid eruption of the Siberian traps flood basalts at the permo-triassic boundary. *Science* **1991**, *253*, 176–179. [[CrossRef](#)]
14. Kamo, S.L.; Czamanske, G.K.; Krogh, T.E. A minimum U-Pb age for Siberian flood-basalt volcanism. *Geochim. Cosmochim. Acta* **1996**, *60*, 3505–3511. [[CrossRef](#)]
15. Kamo, S.L.; Czamanske, G.K.; Amelin, Y.; Fedorenko, V.A.; Davis, D.W.; Trofimov, V.R. Rapid eruption of Siberian flood-volcanic rocks and evidence for coincidence with the Permian-Triassic boundary and mass extinction at 251 Ma. *Earth Planet. Sci. Lett.* **2003**, *214*, 75–91. [[CrossRef](#)]
16. Reichow, M.K.; Pringle, M.S.; Al'Mukhamedov, A.I.; Allen, M.B.; Andreichev, V.L.; Buslov, M.M.; Davies, C.E.; Fedoseev, G.S.; Fitton, J.G.; Inger, S.; et al. The timing and extent of the eruption of the Siberian Traps large igneous province: Implications for the end-Permian environmental crisis. *Earth Planet. Sci. Lett.* **2009**, *277*, 9–20. [[CrossRef](#)]
17. Svensen, H.; Planke, S.; Polozov, A.G.; Schmidbauer, N.; Corfu, F.; Podladchikov, Y.Y.; Jamtveit, B. Siberian gas venting and the end-Permian environmental crisis. *Earth Planet. Sci. Lett.* **2009**, *277*, 490–500. [[CrossRef](#)]
18. Augland, L.E.; Ryabov, V.V.; Vernikovskiy, V.A.; Planke, S.; Polozov, A.G.; Callegaro, S.; Jerram, D.A.; Svensen, H.H. The main pulse of the Siberian Traps expanded in size and composition. *Sci. Rep.* **2019**, *9*, 1–12. [[CrossRef](#)]
19. Zolotukhin, V.V.; Vilenskii, A.M.; Dyuzhikov, O.A. Basalts of Siberian platform. *Novosib. Nauka* **1986**, *245*, 289. (In Russian)
20. Fedorenko, V.; Czamanske, G. Results of new field and geochemical studies of the volcanic and intrusive rocks of the Maymecha-Kotuy area, Siberian flood-basalt province, Russia. *Int. Geol. Rev.* **1997**, *39*, 479–531. [[CrossRef](#)]
21. Ivanov, A.V.; He, H.; Yan, L.; Ryabov, V.V.; Shevko, A.Y.; Palesskii, S.V.; Nikolaeva, I.V. Siberian Traps large igneous province: Evidence for two flood basalt pulses around the Permo-Triassic boundary and in the Middle Triassic, and contemporaneous granitic magmatism. *Earth-Sci. Rev.* **2013**, *122*, 58–76. [[CrossRef](#)]
22. Lyons, J.J.; Coe, R.S.; Zhao, X.; Renne, P.R.; Kazansky, A.Y.; Izokh, A.E.; Kungurtsev, L.V.; Mitrokhin, D.V. Paleomagnetism of the early Triassic Semeitau igneous series, eastern Kazakstan. *J. Geophys. Res. Solid Earth* **2002**, *107*. [[CrossRef](#)]
23. Saunders, A.D.; England, R.W.; Reichow, M.K.; White, R.V. A mantle plume origin for the Siberian traps: Uplift and extension in the West Siberian Basin, Russia. *Lithos* **2005**, *79*, 407–424. [[CrossRef](#)]
24. Vyssotski, A.V.; Vyssotski, V.N.; Nezhdanov, A.A. Evolution of the West Siberian Basin. *Mar. Pet. Geol.* **2006**, *23*, 93–126. [[CrossRef](#)]
25. Buslov, M.M.; Safonova, I.Y.; Fedoseev, G.S.; Reichow, M.; Davies, K.; Babin, G.A. Permo-Triassic plume magmatism of the Kuznetsk Basin, Central Asia: Geology, geochronology, geochemistry, and geodynamic consequences. *Russ. Geol. Geophys.* **2010**, *51*, 322–327. [[CrossRef](#)]
26. Fedorenko, V.A.; Lightfoot, P.C.; Naldrett, A.J.; Czamanske, G.K.; Hawkesworth, C.J.; Wooden, J.L.; Ebel, D.S. Petrogenesis of the flood-basalt sequence at Noril'sk, North Central Siberia. *Int. Geol. Rev.* **1996**, *38*, 99–135. [[CrossRef](#)]
27. Vasil'ev, Y.R.; Zolotukhin, V.V.; Feoktistov, G.D.; Prusskaya, S.N. Evaluation of the volumes and genesis of Permo-Triassic Trap magmatism of the Siberian platform. *Geol. Geofiz.* **2000**, *41*, 1696–1705.
28. Dobretsov, N.L. Mantle plumes and their role in the formation of anorogenic granitoids. *Geol. Geofiz.* **2003**, *44*, 1243–1261.
29. Burgess, S.D.; Bowring, S.A. High-precision geochronology confirms voluminous magmatism before, during, and after Earth's most severe extinction. *Sci. Adv.* **2015**, *1*, e1500470. [[CrossRef](#)]
30. Latyshev, A.V.; Rad'ko, V.A.; Veselovskiy, R.V.; Fetisova, A.M.; Pavlov, V.E. Correlation of the Permian-Triassic ore-bearing intrusions of the Norilsk region with the volcanic sequence of the Siberian Traps based on the paleomagnetic data. *Econ. Geol.* **2020**. [[CrossRef](#)]
31. Gurevitch, E.L.; Heunemann, C.; Rad'ko, V.; Westphal, M.; Bachtadse, V.; Pozzi, J.P.; Feinberg, H. Palaeomagnetism and magnetostratigraphy of the Permian-Triassic northwest central Siberian Trap Basalts. *Tectonophysics* **2004**, *379*, 211–226. [[CrossRef](#)]

32. Steiner, M.B. The magnetic polarity time scale across the Permian-Triassic boundary. *Geol. Soc. Spec. Publ.* **2006**, *265*, 15–38. [[CrossRef](#)]
33. Fetisova, A.M.; Veselovskii, R.V.; Latyshev, A.V.; Rad'ko, V.A.; Pavlov, V.E. Magnetic stratigraphy of the Permian-Triassic traps in the Kotui River valley (Siberian Platform): New paleomagnetic data. *Stratigr. Geol. Correl.* **2014**, *22*, 377–390. [[CrossRef](#)]
34. Riisager, J.; Riisager, P.; Pedersen, A.K. Paleomagnetism of large igneous provinces: Case-study from West Greenland, North Atlantic igneous province. *Earth Planet. Sci. Lett.* **2003**, *214*, 409–425. [[CrossRef](#)]
35. Chenet, A.L.; Fluteau, F.; Courtillot, V.; Gérard, M.; Subbarao, K.V. Determination of rapid Deccan eruptions across the Cretaceous-Tertiary boundary using paleomagnetic secular variation: Results from a 1200-m-thick section in the Mahabaleshwar escarpment. *J. Geophys. Res. Solid Earth* **2008**, *113*, B04101. [[CrossRef](#)]
36. Chenet, A.L.; Courtillot, V.; Fluteau, F.; Gérard, M.; Quidelleur, X.; Khadri, S.F.R.; Subbarao, K.V.; Thordarson, T. Determination of rapid Deccan eruptions across the Cretaceous-Tertiary boundary using paleomagnetic secular variation: 2. Constraints from analysis of eight new sections and synthesis for a 3500-m-thick composite section. *J. Geophys. Res. Solid Earth* **2009**, *114*, B06103. [[CrossRef](#)]
37. Moulin, M.; Courtillot, V.; Fluteau, F.; Valet, J.P. The “Van Zijl” Jurassic geomagnetic reversal revisited. *Geochem. Geophys. Geosyst.* **2012**, *13*, Q03010. [[CrossRef](#)]
38. Heunemann, C.; Krása, D.; Soffel, H.C.; Gurevitch, E.; Bachtadse, V. Directions and intensities of the Earth's magnetic field during a reversal: Results from the Permo-Triassic Siberian trap basalts, Russia. *Earth Planet. Sci. Lett.* **2004**, *218*, 197–213. [[CrossRef](#)]
39. Pavlov, V.E.; Fluteau, F.; Veselovskiy, R.V.; Fetisova, A.M.; Latyshev, A.V. Secular geomagnetic variations and volcanic pulses in the Permian-Triassic traps of the Norilsk and Maimecha-Kotui provinces. *Izv. Phys. Solid Earth* **2011**, *47*, 402–417. [[CrossRef](#)]
40. Pavlov, V.; Fluteau, F.; Veselovskiy, R.; Fetisova, A.; Latyshev, A.; Elkins-Tanton, L.T.; Sobolev, A.V.; Krivolutskaya, N.A. Volcanic pulses in the Siberian Traps as inferred from Permo-Triassic geomagnetic secular variations. In *Volcanism and Global Environmental Change*; Cambridge University Press: Cambridge, UK, 2015; pp. 63–78.
41. Pavlov, V.E.; Fluteau, F.; Latyshev, A.V.; Fetisova, A.M.; Elkins-Tanton, L.T.; Black, B.A.; Burgess, S.D.; Veselovskiy, R.V. Geomagnetic Secular Variations at the Permian-Triassic Boundary and Pulsed Magmatism During Eruption of the Siberian Traps. *Geochem. Geophys. Geosyst.* **2019**, *20*, 773–791. [[CrossRef](#)]
42. Latyshev, A.V.; Veselovskiy, R.V.; Ivanov, A.V. Paleomagnetism of the Permian-Triassic intrusions from the Tunguska syncline and the Angara-Taseeva depression, Siberian Traps Large Igneous Province: Evidence of contrasting styles of magmatism. *Tectonophysics* **2018**, *723*, 41–55. [[CrossRef](#)]
43. Fedorenko, V.; Czamanske, G.; Zen'ko, T.; Budahn, J.; Siems, D. Field and geochemical studies of the melilite-bearing Arydzhangsky suite, and an overall perspective on the Siberian alkaline-ultramafic flood-volcanic rocks. *Int. Geol. Rev.* **2000**, *42*, 769–804. [[CrossRef](#)]
44. Egorov, V.N. Dismemberment and correlation of the Triassic volcanic rocks of the Maimecha-Kotuy province. *Nedra Taymyra Collect. Artic.* **1995**, *1*, 141–154. (In Russian)
45. Shihorina, K.M. Volcanic formations of the Maimecha-Kotuy province. In *SB. Carbonatites and Alkaline Rocks of the North of Siberia (Collection of Articles)*; Leningrad State University: Leningrad, Russia, 1970; pp. 5–14. (In Russian)
46. Ivanov, A.I.; Pirozhnikov, L.P. The age of alkaline ultramafic volcanic rocks of the north of the Siberian Platform. *Dokl. Akad. Nauk. SSSR* **1959**, *127*, 1078–1080.
47. Burgess, S.D.; Bowring, S.; Shen, S.Z. High-precision timeline for Earth's most severe extinction. *Proc. Natl. Acad. Sci. USA* **2014**, *111*, 3316–3321. [[CrossRef](#)] [[PubMed](#)]
48. Gusev, B.V.; Metallova, V.V.; Fainberg, F.S. Magnetizm porod trappovoi formatsii zapadnoi chasti Sibirskoi platformy (Magnetism of Traps in the Western Siberian Craton). *Len Ingrad Nedra* **1967**, *1*, 129. (In Russian)
49. Sidoras, S.D. Magnetism of volcanogenic rocks of the Tunguska syncline and its significance for the geological studies. *Ext. Abstr. Cand. Sci. (Geol. Min.) Diss. Leningr.* **1984**, *1*, 204. (In Russian)
50. Lopatin, G.G.; Nechaev, P.S.; Trofimov, V.R.; Drobotenko, E.A. *State Geological Map 1:200,000 Scale, Sheet R-47-XI,XII. Explanatory Note*; VSEGEI: Saint-Petersburg, Russia, 1996; p. 281.
51. Enkin, R.J. A computer program package for analysis and presentation of paleomagnetic data. *Pac. Geosci. Cent. Geol. Surv. Can.* **1994**, *4*, 16.

52. Chadima, M.; Hrouda, F. Remasoft 3.0 a user-friendly paleomagnetic data browser and analyzer. *Trav. Geophys.* **2006**, *27*, 20–21.
53. Kirschvink, J.L. The least-square line and plane and the analysis of paleomagnetic data. *Geophys. J. R. Astron. Soc.* **1980**, *62*, 699–718. [[CrossRef](#)]
54. Fisher, R. Dispersion on a Sphere. *Proc. R. Soc. A Math. Phys. Eng. Sci.* **1953**, *217*, 295–305. [[CrossRef](#)]
55. Shcherbakova, V.V.; Zhidkov, G.V.; Shcherbakov, V.P.; Latyshev, A.V.; Fetisova, A.M. Verifying the mesozoic dipole low hypothesis by the Siberian trap data. *Izv. Phys. Solid Earth* **2015**, *51*, 362–382. [[CrossRef](#)]
56. McFadden, P.L.; McElhinny, M.W. Classification of the reversal test in palaeomagnetism. *Geophys. J. Int.* **1990**, *103*, 725–729. [[CrossRef](#)]
57. Veselovsky, R.V.; Gallet, Y.; Pavlov, V.E. Paleomagnetism of traps in the Podkamennaya Tunguska and Kotui River Valleys: Implications for the post-Paleozoic relative movements of the Siberian and East European platforms. *Izv. Phys. Solid Earth* **2003**, *39*, 78.
58. Gapeev, A.K.; Gribov, S.K. Magnetic properties of intrusive traps of the Siberian platform: Evidence for a self-reversal of the natural remanent magnetization. *Izv. Phys. Solid Earth* **2008**, *44*, 822–838. [[CrossRef](#)]
59. Shcherbakov, V.P.; Latyshev, A.V.; Veselovskiy, R.V.; Tselmovich, V.A. Origin of false components of NRM during conventional stepwise thermal demagnetization. *Russ. Geol. Geophys.* **2017**, *58*, 1118–1128. [[CrossRef](#)]
60. Mel'nikov, B.N.; Khisina, N.R. Spinodal Decomposition and the Related Partial Self-Reversal of Magnetization in Titanomagnetites of African Rift Zones. *Izv. Akad. Nauk. SSSR Fiz. Zemli* **1976**, *10*, 84–92.
61. Krása, D.; Shcherbakov, V.P.; Kunzmann, T.; Petersen, N. Self-reversal of remanent magnetization in basalts due to partially oxidized titanomagnetites. *Geophys. J. Int.* **2005**, *162*, 115–136. [[CrossRef](#)]
62. Mikhaltsov, N.E.; Kazansky, A.Y.; Ryabov, V.V.; Shevko, A.Y.; Kuprish, O.V.; Bragin, V.Y. Paleomagnetism of trap basalts in the northwestern Siberian craton, from core data. *Russ. Geol. Geophys.* **2012**, *53*, 1228–1242. [[CrossRef](#)]
63. Latyshev, A.V.; Ulyakhina, P.S.; Krivolutskaya, N.A. Signs of the Record of Geomagnetic Reversal in Permian—Triassic Trap Intrusions of the Ergalakhsky Complex, Norilsk Region. *Izv. Phys. Solid Earth* **2019**, *55*, 270–286. [[CrossRef](#)]
64. Lind, E.N.; Kropotov, S.V.; Czamanske, G.K.; Grommé, S.C.; Fedorenko, V.A. Paleomagnetism of the Siberian Flood Basalts of the Noril'k Area: A Constraint on Eruption Duration. *Int. Geol. Rev.* **1994**, *36*, 1139–1150. [[CrossRef](#)]
65. Veselovskiy, R.V.; Konstantinov, K.M.; Latyshev, A.V.; Fetisova, A.M. Paleomagnetism of the trap intrusive bodies in arctic Siberia: Geological and methodical implications. *Izv. Phys. Solid Earth* **2012**, *48*, 738–750. [[CrossRef](#)]
66. Hounslow, M.W.; Muttoni, G. The geomagnetic polarity timescale for the Triassic: Linkage to stage boundary definitions. *Geol. Soc. Spec. Publ.* **2010**, *334*, 61–102. [[CrossRef](#)]
67. Hounslow, M.W.; Balabanov, Y.P. A geomagnetic polarity timescale for the Permian, calibrated to stage boundaries. *Geol. Soc. Lond. Spec. Publ.* **2018**, *450*, 61–103. [[CrossRef](#)]
68. Ogg, J.; Ogg, G.; Gradstein, F. *A Concise Geologic Time Scale*; Elsevier: Amsterdam, The Netherlands, 2016.
69. Hounslow, M.W. Geomagnetic reversal rates following Palaeozoic superchrons have a fast restart mechanism. *Nat. Commun.* **2016**, *7*, 1–13. [[CrossRef](#)] [[PubMed](#)]
70. Miller, J.S.; Matzel, J.E.P.; Miller, C.F.; Burgess, S.D.; Miller, R.B. Zircon growth and recycling during the assembly of large, composite arc plutons. *J. Volcanol. Geotherm. Res.* **2007**, *167*, 282–299. [[CrossRef](#)]
71. Schaltegger, U.; Davies, J.H.F.L. Petrochronology of Zircon and Baddeleyite in Igneous Rocks: Reconstructing Magmatic Processes at High Temporal Resolution. *Rev. Miner. Geochem.* **2017**, *83*, 297–328. [[CrossRef](#)]
72. Distler, V.V.; Kunilov, V.E. Geology and ore deposits of the Noril'sk region. In *VII International Platinum Symposium Guidebook*; Moskovskiy Contact: Moscow, Russia, 1994; p. 67.
73. Rad'ko, V.A. Model of dynamic differentiation of Intrusive traps of the North-West Siberian platform. *Geol. Geophys.* **1991**, *11*, 19–27.
74. Naldrett, A.J. *Magmatic Sulfide Deposits of Nickel-Copper and Platinum-Metal Ores*; St. Petersburg University: St. Petersburg, Russia, 2003; p. 487.
75. Lightfoot, P.C.; Hawkesworth, C.J.; Hergt, J.; Naldrett, A.J.; Gorbachev, N.S.; Fedorenko, V.A.; Doherty, W. Remobilisation of the continental lithosphere by mantle plumes: Major-/trace-element and Sr-, Nd-, and Pb-isotope evidence from picritic and tholeiitic lavas of the Noril'sk district, Siberian Trap, Russia. *Contrib. Miner. Petrol.* **1993**, *114*, 171–188. [[CrossRef](#)]
76. Al'mukhamedov, A.I.; Medvedev, A.Y.; Zolotukhin, V.V. Chemical evolution of the permian-triassic basalts of the siberian platform in space and time. *Petrology* **2004**, *12*, 297–311.

77. Westphal, M.; Gurevitch, E.L.; Samsonov, B.V.; Feinberg, H.; Pozzi, J.P. Magnetostratigraphy of the lower Triassic volcanics from deep drill SG6 in western Siberia: Evidence for long-lasting Permo-Triassic volcanic activity. *Geophys. J. Int.* **1998**, *134*, 254–266. [[CrossRef](#)]
78. Glen, J.M.G.; Nomade, S.; Lyons, J.J.; Metcalfe, I.; Mundil, R.; Renne, P.R. Magnetostratigraphic correlations of Permian-Triassic marine-to-terrestrial sections from China. *J. Asian Earth Sci.* **2009**, *36*, 521–540. [[CrossRef](#)]
79. Naumov, V.A.; Ankudimova, L.A. Palynocomplexes and age of volcanogenic deposits of the Angara Katanga Area (Middle Angara Region). *Geol. Geofiz.* **1995**, *36*, 39–45.
80. Latyshev, A.V.; Veselovskiy, R.V.; Ivanov, A.V.; Fetisova, A.M.; Pavlov, V.E. Short Intense Bursts in Magmatic Activity in the South of Siberian Platform (Angara Taseeva Depression): The Paleomagnetic Evidence. *Izv. Phys. Solid Earth* **2013**, *49*, 823–835. [[CrossRef](#)]
81. Gurevitch, E.; Westphal, M.; Daragan-Suchov, J.; Feinberg, H.; Pozzi, J.P.; Khramov, A.N. Paleomagnetism and magnetostratigraphy of the traps from Western Taimyr (northern Siberia) and the Permo-Triassic crisis. *Earth Planet. Sci. Lett.* **1995**, *136*, 461–473. [[CrossRef](#)]
82. Kazansky, A.Y.; Metelkin, D.V.; Bragin, V.Y.; Kungurtsev, L.V. Paleomagnetism of the Permian and Triassic traps from the Kuznetsk Basin (southern Siberia). *Geol. Geofiz.* **2005**, *46*, 1107–1120.
83. Ross, P.S.; Ukstins Peate, I.; McClintock, M.K.; Xu, Y.G.; Skilling, I.P.; White, J.D.L.; Houghton, B.F. Mafic volcanoclastic deposits in flood basalt provinces: A review. *J. Volcanol. Geother. Res.* **2005**, *145*, 281–314. [[CrossRef](#)]
84. Black, B.A.; Weiss, B.P.; Elkins-Tanton, L.T.; Veselovskiy, R.V.; Latyshev, A. Siberian Traps volcanoclastic rocks and the role of magma-water interactions. *Bull. Geol. Soc. Am.* **2015**, *127*, 1437–1452. [[CrossRef](#)]
85. Jerram, D.A.; Svensen, H.H.; Planke, S.; Polozov, A.G.; Torsvik, T.H. The onset of flood volcanism in the north-western part of the Siberian Traps: Explosive volcanism versus effusive lava flows. *Palaeogeogr. Palaeoclim. Palaeoecol.* **2016**, *441*, 38–50. [[CrossRef](#)]
86. Ganino, C.; Arndt, N.T. Climate changes caused by degassing of sediments during the emplacement of large igneous provinces. *Geology* **2009**, *37*, 323–326. [[CrossRef](#)]
87. Burgess, S.D.; Muirhead, J.D.; Bowring, S.A. Initial pulse of Siberian Traps sills as the trigger of the end-Permian mass extinction. *Nat. Commun.* **2017**, *8*, 164. [[CrossRef](#)]
88. Elkins-Tanton, L.T.; Grasby, S.E.; Black, B.A.; Veselovskiy, R.V.; Ardakani, O.H.; Goodarzi, F. Field evidence for coal combustion links the 252 Ma Siberian Traps with global carbon disruption. *Geology* **2020**. [[CrossRef](#)]
89. Xie, S.C.; Pancost, R.D.; Yin, H.F.; Wang, H.M.; Evershed, R.P. Two episodes of microbial change coupled with Permo/Triassic faunal mass extinction. *Nature* **2005**, *434*, 494–497. [[CrossRef](#)]
90. Song, H.J.; Wignall, P.B.; Tong, J.N.; Yin, H.F. Two pulses of extinction during the Permian—Triassic crisis. *Nat. Geosci.* **2013**, *6*, 52–56. [[CrossRef](#)]
91. Huang, Y.; Chen, Z.-Q.; Algeo, T.J.; Zhao, L.; Baud, A.; Bhat, G.M.; Zhang, L.; Guo, Z. Two-stage marine anoxia and biotic response during the Permian-Triassic transition in Kashmir, northern India; pyrite framboid evidence. *Glob. Planet. Chang.* **2019**, *172*, 124–139. [[CrossRef](#)]
92. Martindale, R.C.; Foster, W.J.; Velledits, F. The survival, recovery, and diversification of metazoan reef ecosystems following the end-Permian mass extinction event. *Palaeogeogr. Palaeoclimatol. Palaeoecol.* **2019**, *513*, 100–115. [[CrossRef](#)]
93. Szurlies, M.; Geluk, M.C.; Krijgsman, W.; Kürschner, W.M. The continental Permian-Triassic boundary in the Netherlands: Implications for the geomagnetic polarity time scale. *Earth Planet Sci. Lett.* **2012**, *317/318*, 165–176. [[CrossRef](#)]
94. Szurlies, M. Late Permian (Zechstein) magnetostratigraphy in Western and Central Europe. *Geol. Soc. Spec. Publ.* **2013**, *376*, 73. [[CrossRef](#)]
95. Mundil, R.; Ludwig, K.R.; Metcalfe, I.; Renne, P.R. Age and timing of the Permian mass extinctions: U/Pb dating of closed-system zircons. *Science* **2004**, *305*, 1760–1763. [[CrossRef](#)]
96. Shen, S.Z.; Crowley, J.L.; Wang, Y.; Bowring, S.A.; Erwin, D.H.; Sadler, P.M.; Cao, C.Q.; Rothman, D.H.; Henderson, C.M.; Ramezani, J.; et al. Calibrating the end-Permian mass extinction. *Science* **2011**, *334*, 1367. [[CrossRef](#)]

